Zlotnicki *et al. Earth, Planets and Space (2018) 70:159*
https://doi.org/10.1186/s40623-018-0925-2

Earth, Planets and Space

FULL PAPER

Open Access

The 2010 seismovolcanic crisis at Taal Volcano (Philippines)

Jacques Zlotnicki[1*], Y. Sasai[2], M. J. S. Johnston[3], F. Fauquet[1], E. Villacorte[4] and J. M. Cordon Jr.[4]

Abstract

Typical eruptions of Taal Volcano in the Philippines are frequent and violently explosive. The last devastating phreatomagmatic eruption from 1965 to 1977 resulted in the death of about 200 persons. For this and other earlier events, no warnings of impending eruptions were issued. Since this time, volcanic crises involving episodes of seismicity, deformation, gas release, temperature change, etc., have occurred frequently.Each of these did not, but possibly could have, evolved into an explosive eruption. One such event occurred between April 2010 and March 2011. This paper reports various types of geophysical data (electric/magnetic field, ground temperature, seismicity and ground deformation) taken during this period of activity together with the current state of geophysical knowledge about the volcano in order to throw light on activity evolution. While the 2010 seismovolcanic crisis was preceded by unusual changes in electric field, ground tilting and uplift, the major signals from all data were concomitant with the evolution of the crisis. On April 20, 2010, felt earthquakes first started to occur. The numbers increased sharply after April 29 with repeated pulses of seismicity that ended finally in March 2011. Overall, we can identify three periods of seismic activity, from April 20 to August 4–8, from August 4–8 to November 18, and from November 18 to March 28, 2011. Although only a single tiltmeter was in operation, it recorded three phases of deformation that correspond generally with the pulses in seismic activity. Phase 1 appears to correspond to inflation at a depth of about 5 km just to the NW of Main Crater Lake from April 20 to June 11, 2010. This resulted in an eastward tilting of the northern flank of the volcano. This apparently triggered rapid but shallower inflation (Phase 2) in the hydrothermal region of the volcano under the northern edge of Main Crater Lake from June 11 to July 13 just to the SE of the initial deeper source as indicated by northward tilting of the volcano's northern flank. Progressive deflation began after July 13. By March 28, 2011, the deformation state recovered to the pre-crisis level and felt seismic activity ceased. Apparent related changes in seismicity, tilt, magnetic and electric fields occur during smaller NS inflations in the Phase 3 deflation—Phase 3a (July 13 to August 4–8), Phase 3b (August 4–8 to November 18) and Phase 3c (November 18 to March 28, 2011). These likely result from interrelated stress change, fluid/gas migration and thermal activity at depth and in the hydrothermal system. The rapidity of changes in the state of the volcano over a matter of hours during this entire process indicates rapid communication occurs between processes at depth and in the hydrothermal system and this could easily result in the dramatic evolution to violent phreatic explosions with little warning.

Keywords: Taal Volcano, Multi-parameters monitoring, Tilt, Seismicity, Electromagnetism, Electricity, 2010 crisis, Volcanic risk

*Correspondence: jacques.zlotnicki@wanadoo.fr
[1] CNRS, OPGC-UMR6524, 24 av des Landais, 63171 Aubière Cedex, France
Full list of author information is available at the end of the article

Introduction

Taal Volcano is a huge active stratovolcano, located at the southwestern end of the Macolod corridor in the large convergence zone between the Eurasian and Philippine tectonic plates (Fig. 1a) (Galgana et al. 2007). The currently activity is confined to Volcano Island in the center of an older water-filled caldera about 25–30 km in diameter that last erupted about 5000–7000 years B.P. (Ohkura et al. 2001; Ramos 2002; Galgana et al. 2007). Resurgent volcano growth that formed Volcano Island together with eruptions of large volumes of ash (e.g., 1749, 1754) and weak tectonic uplift have combined to progressively isolate the older caldera from the China Sea (Maso 1991; Ramos 2002; http://www.iml.rwth-aachen.de/Petrographie/taal-mas/ta-maso.htm).

Volcano Island is now a 5-km wide, 311 m high, resurgent dome within the older caldera that is now filled with fresh water to a depth of about 180 m thereby forming Taal Lake ("TL" hereafter). At the top of Volcano Island, a smaller central crater lake with a diameter of about 1.2 km has formed (Fig. 1b). This 75 m deep acidic lake, called Main Crater Lake ("*MCL*" hereafter), has an average water temperature of 33 °C (Fig. 2) (see also Arpa et al. 2013).

Eruptions on Taal can be powerful and violent. Phreatic, phreatomagmatic, plinian and strombolian eruptions possibly accompanied by pyroclastic surges and large ash clouds may happen with little warning, and until now, no eruptions have been forecast well in advance. Volcanic Explosivity Indices [VEI (Newhall and Self 1982)] can be high as 4, as for the 1716, 1749, 1754, and 1965 eruptions (http://www.volcano.si.edu/volcano.cfm?vn=273070; Zlotnicki et al. 2017). To put this in perspective, ash clouds reached Manila metropolitan city during the 1911 eruption for which the VEI was only equal to 3 (http://volcano.si.edu/volcano.cfm?vn=273070).

The dynamics of the eruptions are apparently controlled by interactions between a magma reservoir (and escaping hot gases and fluids) with ground water from the China Sea, Taal Lake and the Main Crater Lake in addition to the seasonal rainfall (about 5 m/y) (Delmelle et al. 1998). Considerable evapotranspiration associated with powerful hydrothermal dynamics results in thermal transfer and mineralization of solid rocks through active fissures, geyser activity and fumarole activity in the upper part of the volcano (Cardenas et al. 2012). These processes mechanically weaken the different lithologies

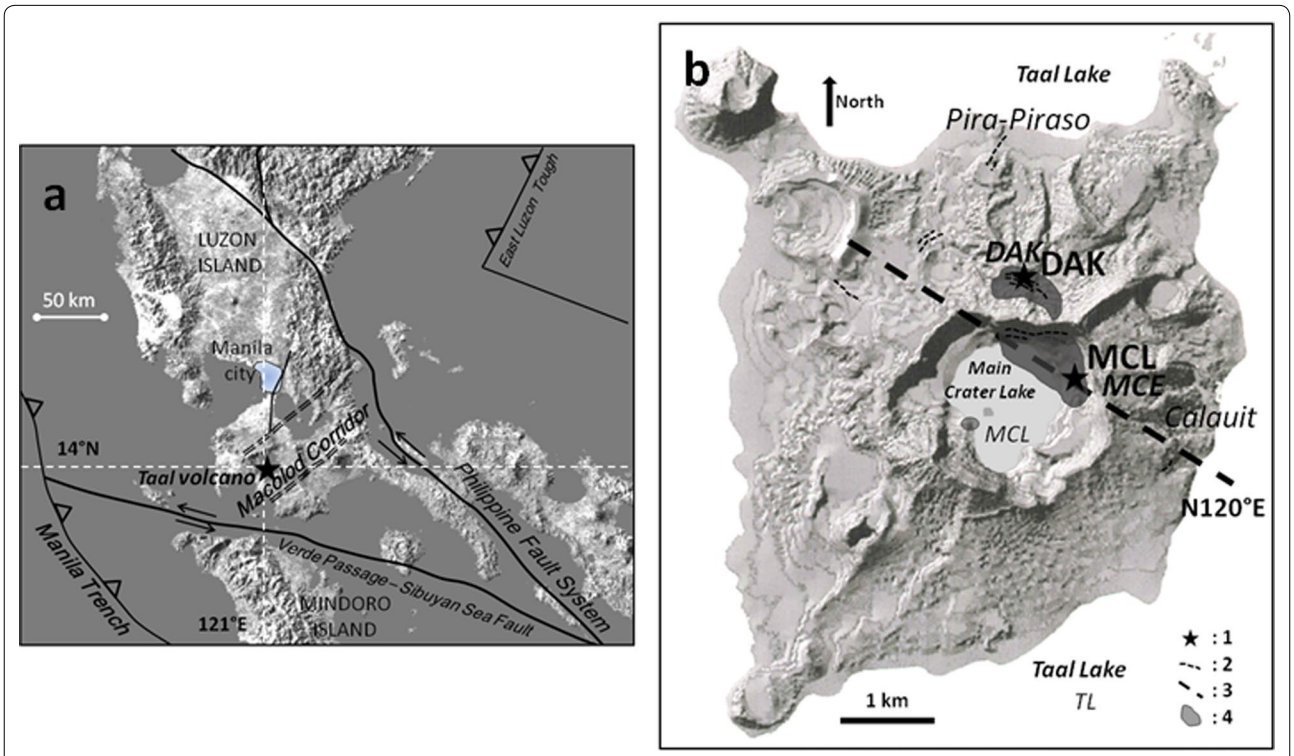

Fig. 1 **a** Schematic of the tectonics near Luzon Island in the Philippines archipelago. The location of Taal Volcano is marked by a black star. **b** Topographic map of the Volcano Island. *1* Stars show multi-parameters stations DAK and MCL; *DAK* and *MCE* are self-recording total field magnetometers; *2* Small dashed lines are fissures; *3* Dashed line shows the N120°E regional tectonic axis along which major hydrothermal activity takes place; *4* Dark gray areas show permanent geothermal fields defined by surface activity, higher heat flow and degassing fluxes

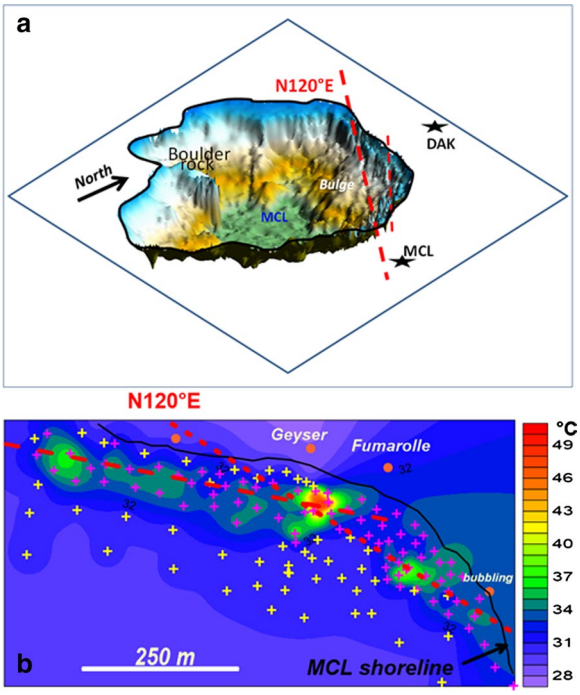

Fig. 2 **a** Bathymetry of Main Crater Lake (*MCL*); Red axis corresponds to the main submarine fissure axis (N120°E, heavy dashed line) along which degassing and heat fluxes are predominant. A secondary fissure is shown as a thin-dashed red line. **b** Thermal anomalies at the bottom of *MCL* recognized in December 2009 (pink crosses) and March 2010 (yellow crosses). Red dashed lines are fissures depicted in **a**

of the volcanic edifice. Major sources of CO_2 degassing emanate from the magmatic source(s), geothermal areas, active fissures, and the *MCL* (Zlotnicki et al. 2009b; Pérez et al. 2011; Maussen et al. 2018). The CO_2 flux can be on the order of 500 t/d during quiet periods and can reach as much as 4000 t/d during large seismic activity (Arpa et al. 2013; A. Bernard personal communication). Most of these features arise from a large hydrothermal region overlying deeper magmatic bodies (Delmelle et al. 1998; Zlotnicki et al. 2009a, 2017; Fikos et al. 2012; Yamaya et al. 2013; Alanis et al. 2013).

In particular till 2010, strong CO_2 degassing and high heat flow occurs along east–west orientated fissures just to the north of *MCL* till Daang Kastila area ("DAK") (Fig. 1b). Other sets of small fissures showing high heat flow occurred on the outer northern flank of the crater and along the northern shoreline of Taal Lake during large seismic crises (1992–1994) ("Pira-Piraso and Calauit districts") (Fig. 1b). (Harada et al. 2005; Zlotnicki et al. 2009a, b). These fissure areas are apparently linked at depth as shown by 13 audio-magnetotelluric soundings made in 2007 along a north–south cross section of the volcano (Zlotnicki et al. in preparation) and by the apparent resistivity mapping of this region of the volcano [Fig. 3a(a), a(b)] (Fikos et al. 2012).

The bottom topography of *MCL* shows fissures striking N120°E at the bottom of the Lake through which intense fluxes of hot gases are passing (Figs. 2a, b, 3a). These fissures are particularly apparent in a bulge of about 1 Mm^3 under the north part of the lake (Fig. 2a). Most likely, this bulge appeared during the 1992 and 1994 seismic crises since extensions of these fissures opened on land and in the cliff forming the crater rim at this time. Further to the east, fissuring progressively decreases, bends to the southeast and disappears before reaching the crater rim.

The deep resistivity structure was determined using wideband magnetotelluric sounding surveys (Fig. 3c). The 2-D modeling results (Yamaya et al. 2013) show a zone of higher resistivity beneath the *MCL* that apparently extends downward from about 0.5 km to about 4 km depth. In this central zone, located at about 2.5 km depth, the resistivity has values between 20 and 100 Ohm m as compared to values smaller than 10 Ohm m outside the zone. The results from 3-D modeling of the resistivity structure (Alanis et al. 2013) identify the location and the shape of the hydrothermal reservoir beneath around the center of *MCL* to be approximately 3 km wide and centered at about 2.5 km depth. This zone could correspond to the part of the hydrothermal system where temperatures exceed 200 °C. Both Yamaya et al. (2013) and Alanis et al. (2013) concluded that the magmatic body indicated by GPS networks is likely at a depth between 4 and 6 km under *MCL* (Lowry et al. 2001; Bartel et al. 2003; Galgana et al. 2014).

Since 1572, 33 historical eruptions have been identified. The most recent violent phreatomagmatic eruption began in 1965 and ended in 1977. This produced pyroclastic flows that reached as far as the southwestern rim of the old caldera (Moore et al. 1966). Since that time, activity has been characterized by episodes of deformation and seismicity without surface eruptive products. Such active periods occurred in 1992 with up to 2550 felt events per day and during 1994 with up to 1550 felt earthquakes per day, respectively. During this time, inflation reached 16 cm at DAK and about 10 cm near Calauit to the southeast and the temperature of the *MCL* rose to 39–41 °C (Lowry et al. 2001; Bartel et al. 2003; Galgana et al. 2014).

Since 1994, periods of inflation occurred in February–November 2000 and in June 2004–March 2005 when extension rates of 145 mm yr^{-1} and uplift rates of 220 mm yr^{-1} were observed by Bartel et al. (2003) and Galgana et al. (2014) with no obvious correspondence between deformation and seismicity. The authors fit these deformation data with simple point-source Mogi models and finite-element models for elastic and viscoelastic

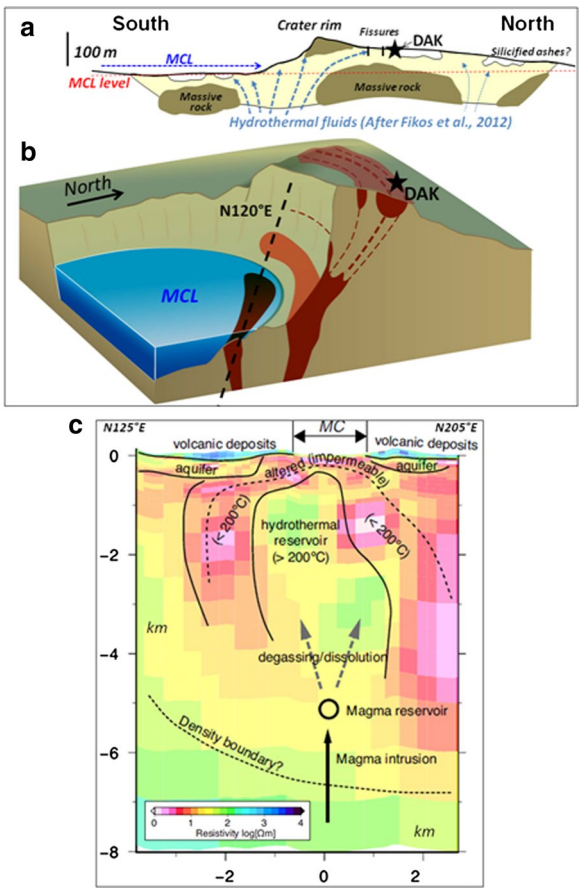

Fig. 3 **a** Sketch of the geological structure and the hydrothermal circulation deduced from the inversion of Electrical Resistivity Tomography (after Fikos et al. 2012). **b** General pattern of the geothermal fields in 2010. Brown areas correspond to permanent geothermal fields (after Zlotnicki et al. 2009a). **c** Inversion of 2D and 3D deep magnetotelluric soundings (after Yamaya et al. 2013; Alanis et al. 2013)

material and concluded that the deformation could have been generated by a change in pressure (or volume) of a source at a depth of about 5 km beneath Daang Kastila (DAK—Fig. 1b) in 2000, and under the eastern shore of *MCL* (MCL—Fig. 2a) in 2005. It is consistent with the concept of episodic inflation phases being caused by intermittent intrusions of magma into a shallow reservoir of magma at about 5 km depth and deflation phases caused by exsolution of magmatic fluids and gases into an overlying unconfined, but not yet identified at that time, hydrothermal system.

After the large seismic crisis in early 2005, during which some hundreds of inhabitants' spontaneously evacuated Volcano Island for a few days, the seismicity decreased. Occasional minor swarms did occur over several weeks each year. In spite of decreasing seismicity, the Philippines Institute of Volcanology and Seismology (PHIVOLCS, http://www.phivolcs.dost.gov.ph/) recorded leveling data that showed persistent low and gradual inflation of the volcano with largest amplitudes on the west/northwest sector. The maximum uplift reached 18 mm along the western survey line between 2005 and mid-2010.

In summary, the present day knowledge of the structure within Taal Volcano indicates:

1. A steady state magmatic source of unknown shape may be located between 4 and 6 km depth below the *MCL* (Zlotnicki et al. 2017). Its exact location is not well constrained, and it may migrate with time, oscillating from the northern flank to the inner northern part of the *MCL*.
2. High gas flow and volcanic fluids emanate from this magma reservoir and contribute to the activity of the hydrothermal system located directly above the reservoir under the *MCL*.
3. At depths shallower than about 2 km, the hydrothermal system vents either into the northern part of the crater where higher gas concentrations and thermal fluxes are observed or into the 400 m long fissures system on the north flank that apparently opened during the 1992 and 1994 deformational and seismic swarm crises. In both of these areas, regions of high heat flux are observed and are reactivated during periods of sporadic deformation and seismic activity.

In 2005, The international Inter-Association on Electromagnetic Studies of Earthquakes and Volcanoes (EMSEV, http://www.emsev-iugg.org/emsev/), in cooperation with PHIVOLCS joined together in an effort to provide repeat surveys and continuous monitoring of many geophysical parameters on Taal Volcano. Real-time monitoring of many of these parameters was provided through continuous telemetry back to the PHIVOLVCS Buco Observatory located on the northern shore of TL. This paper concerns observations, comparisons, possible physical explanations and implications obtained from data prior to and during the most recent seismovolcanic crisis on Taal Volcano in 2010–2011.

Instrumentation

Multi-parameter installations

Construction of the first multi-parameter installation was started in 2005 at Daang Kastila (DAK) near the fissures field on the northern flank of the volcano (Fig. 1b). At this site, a self-recording proton magnetometer *DAK* monitoring the total intensity of the magnetic field (TMF) with a sampling rate of 1/min and resolution of 0.1 nT was installed together with two horizontal components of the electric field obtained from two 127 and

44-m long NS and EW lines with buried non-polarized Pb-$PbCl_2$ electrodes. A seismometer monitoring RMS (root mean square) seismic noise activity, ground temperature sensors set up along the electric lines and a self-leveling borehole insulated tiltmeter supplied by the US Geological Survey were all operational by early March 2010. The ground temperature sensors were installed at depths of 40 and 80 cm. The tiltmeter was installed in a 1-m deep borehole and provide continuous data on the NS and EW components of tilt at a resolution of less than 0.01 μrad. The daily variation in temperature at the sensor is less than 0.1 °C. The tiltmeter, its installation and the telemetry were calibrated together using ocean-load corrected solid earth tides. All data except the total field magnetic data are sampled on an 8-channel 24-bit data logger DAK every 2 s and are telemetered in real-time to the PHIVOLCS Buco Observatory.

The second recording site (MCL) was established to the east of *MCL* (Fig. 1b). A second proton magnetometer *MCE* was installed close to a 3-component fluxgate magnetometer (resolution 0.01 nT) installed in an insulated cavity in the ground. Two NS and EW horizontal electric dipoles of lengths 87 and 81 m were connected to non-polarized Pb-$PbCl_2$ electrodes buried at about 80 cm depth. Ground temperature sensors were also installed at 40 and 80 cm depths with these electrodes and in the center of the array. The eight channels of data were simultaneously recorded every 2 s on an 8-channel 24-bit data logger. Finally, a third data logger was set up on a large boulder rock that protrudes above water surface in the *MCL* to record the water level and temperature of the *MCL*. Water level and temperature data were sampled every 15 min. Unfortunately, the water level recorder has not worked well. The stability of the electrodes was routinely checked with periodic ground surface measurements (Ladanivskyy et al. 2017). Repeat surveys of self-potential, temperature, differential magnetic field, and leveling were made approximately biannually to provide better information on spatial variations.

Background seismicity, uplift and temperature data: January 2005 to January 2010

During this period, the PHIVOLCS seismic network consisted of a few single-component vertical seismic stations that were used primarily for the determination of the daily rate of volcanic earthquakes. From 2005 to 2010, Taal Volcano regularly exhibited minor seismic swarms that decreased in severity (Fig. 4). However, during some of these seismic swarms PHIVOLCS raised the volcano alert level to 1 on a 5-level scale, meaning that

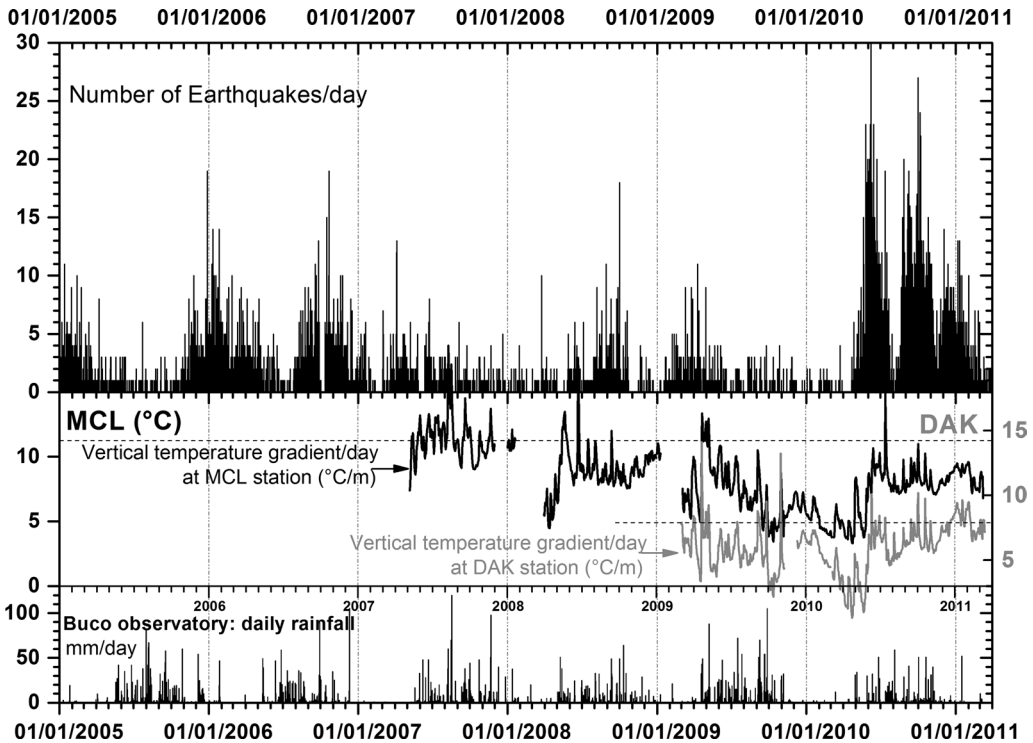

Fig. 4 Top: Daily number of volcanic earthquakes recorded by local Buco Observatory (PHIVOLCS personal communication) between January 2005 and March 2011. Middle: Normalized vertical gradient of ground temperature measured between 40 and 80 cm depth at MCL (black) and DAK (gray) stations. Bottom: Daily rainfall measured at Buco local observatory located at 8 km from Taal crater

low to moderate level of seismicity, ground deformation, increase in ground and water temperatures and increase in bubbling and/or fumarolic activity were being observed. During 2009 and early 2010, seismic activity was generally low. From July to October 2009, a continuous decrease in the ground temperature gradient of 3 °C/m per year was measured at the MCL station with some indications of a similar decrease at DAK. This was followed by variations of 2 °C/m at both sites from October 2009 to the start of the seismic crisis in April 2010.

Repeat measurements of three level lines from the TL shoreline on Volcano Island were made by the PHIVOLCS team approximately biannually after 1999 although more frequently during periods of activity. Just one of these lines (north flank) goes from the shoreline to the crater rim. No noticeable changes were observed on the northern flank between 1999 and 2004. Widespread uplift became more evident after January 2005 and between 2005 and mid-2007 with maximum changes of 12 mm, 15 and 6 mm measured along the west, north and southwest radial uphill lines, respectively (M. Lendio personal communication). Simple modeling suggests this uplift could be produced by a pressure or volume change located at a depth of about 5 km under the *MCL* near the northwestern border of the crater rim. From 2007 to 2010, the deformation remained constant or slightly decreased until the end of March 2010 when it increased sharply.

Other background geophysical data: January 2008 to April 2010

Prior to mid-2009, the horizontal components of the electric fields at DAK and MCL remained on their respective long-term trends, showing only occasional changes less than 200 mV/km in amplitude. Some are apparently linked to changes in the ground temperature and rainfall (Fig. 5) and some are not. From mid-2009, the NS components at both DAK and MCL increased then systematically decreased until early 2010. The EW components did the opposite. Note that NS component of the electric field at DAK is inverted (SN) and is drawn at the top of all data plots in Figs. 5 and 6 for easier comparison with the other records during the crisis.

Figure 6 shows daily records between January 2010 and March 2011 of the horizontal north–south and east–west components of electric fields at DAK and MCL stations, the total magnetic field differences between stations *DAK* and *MCE* and the Muntinlupa magnetic Observatory *MUT*, located at 30 km north from the volcano, as well as local magnetic differences between *MCE* and *DAK* stations, ground temperature at 80 cm depth at DAK and MCL, daily number of earthquakes provided by PHIVOLCS, and daily rainfall at Buco Observatory. Dashed lines through the various parameters are derived from the quiet periods of data during 2008 to mid-2009.

Daily values of the total magnetic field differences [*MCE-DAK*] are remarkably constant during 2008 and early 2009. No changes at *MCE* and *DAK* apparently occurred during this time since the differences [*MCE-MUT*] and [*DAK-MUT*], obtained using the reference station *MUT* some 30-km from Taal, are also constant in spite of some gaps in the data. Although only sparse data were available in TMF from early 2009 to January 2010, the difference [*MCE-DAK*] decreased by 0.5 nT in June 2009 and by 1.8 nT in December 2009. These changes appear confined to the *MCE* since the difference [*DAK-MUT*] remained constant. The magnetic field difference data [*DAK-MUT*] remained relatively flat from early October 2009 to July 13, 2010, implying that little change was observed at *DAK* during the initial stages of the 2010 crisis.

To quantify rainfall effects in the electric and magnetic field data, we compare daily rainfall (bottom plot on Fig. 5) with these data (upper plots on Fig. 5) and also look in detail at any daily rainfall events of more than 50 mm that are plotted on each of the electric and magnetic field axis. By comparing rainfall and magnetic data during 2009 when the seasonal rainfall on Taal Volcano was significantly more than in previous years and in 2010 (Fig. 5) (2007: 1445 mm, 2008: 1218 mm, 2009: 1959 mm, 2010: 1120 mm), it is clear that rainfall does not (and should not) produce any effects in the absolute magnetic field data. In the electric field data, rainfall effects in 2009, if they occur, are transient in nature and decay quickly (days). Examples are seen at DAK with large rainfalls such as the large May 8, 2009 rainfall (88 mm) and during the typhoon on September 27, 2009 (105 mm). The issue is clearly complex since similar longer-term changes occur at other times not related to rainfall (e.g., late July, September, early December) and dominate the small effects at times of large rainfall.

The April 2010–March 2011 seismovolcanic crisis

Seismicity

Seismic swarm activity started on April 20, 2010, and rose sharply after April 29 to result eventually in the highest seismicity episode since the mid-1990s. The three main periods of increased seismicity are apparent in Figs. 5 and 6. During the first period (Period I, April 20 to August 4–8), a peak rate of 32 earthquakes per day occurred on June 8 but by August 4 the seismicity had almost ceased. A second episode started on August 8 (Period II, August 4–8 to November 18). A peak rate of 27 earthquakes occurred on October 1 but returned to background levels by November 18. Finally, a third smaller seismic swarm was observed between

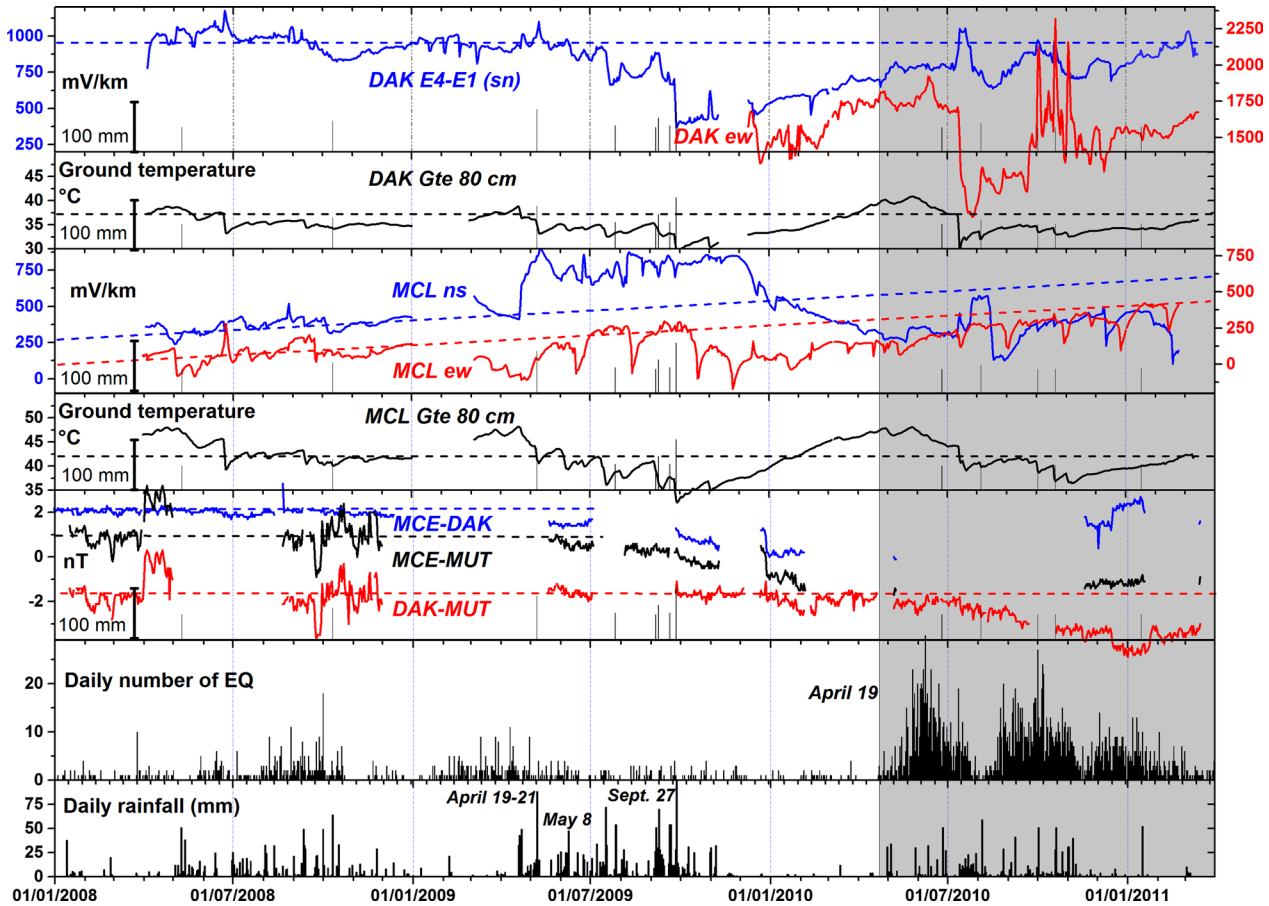

Fig. 5 Daily variations of different parameters between January 2008 and March 2011. Gray box corresponds to the 2010 seismovolcanic crisis. From top to bottom: Horizontal components of the electric field at DAK (S–N, E–W), ground temperature measured at 80 cm depth at DAK, Horizontal components of the electric field at MCL station (N–S, E–W), Ground temperature recorded at 80 cm depth at MCL, Total Magnetic field differences [*DAK–MCE*], [*MCE–MUT*], and [*DAK–MUT*], Daily number of earthquakes (PHIVOLCS document), and Daily rainfall at the local Buco Observatory. Rainfall above 50 mm is added to each plot for comparison with single parameters. Dashed lines correspond to the pre-crisis trends

November 18 and March 2011 (Period III, November 18 to March 2011). The three periods of seismic activity, each lasting about 3.5 months, resulted in a total of about 3000 felt earthquakes. This number is comparable to the total number of earthquakes recorded in the five-year period between 2005 and March 2010.

Long-period (LP) earthquakes usually associated with fluid oscillation in cracks (Chouet 1992; Julian 1994) first appeared after June 2. During the next few weeks, earthquakes with intensities between I and III were felt until July 2. A Level 1 Volcano Alert was first announced by PHIVOLCS on April 29. This was increased to Level 2 on June 8. The level 2 Alert required evacuation of elderly and young people from Volcano Island. The Alert Level was lowered back to 1 on August 2, 2010, and remained here until March 2011.

Level lines

Uplift of 10.3 mm, 11 mm, and 10 mm was observed from January to July 2010 along the west, north and southwest lines, respectively (see line locations in Fig. 9a) (PHIVOLCS personal communication).

Ground tilt recorded on the north flank

The NS and EW components of tilt at DAK monitor tilt of the volcano (Fig. 1b) in approximately radial and tangential directions using a tilt convention where positive tilts are down toward the north and the east, respectively. During the few weeks following the installation, the tiltmeter exhibited an initial tilt toward the south (i.e., toward the volcano and its crater lake) (Fig. 6).

Small transient changes occurred before the first onset of seismicity, but the first spectacular transient signals of various types were observed on April 29 (Fig. 7a). From

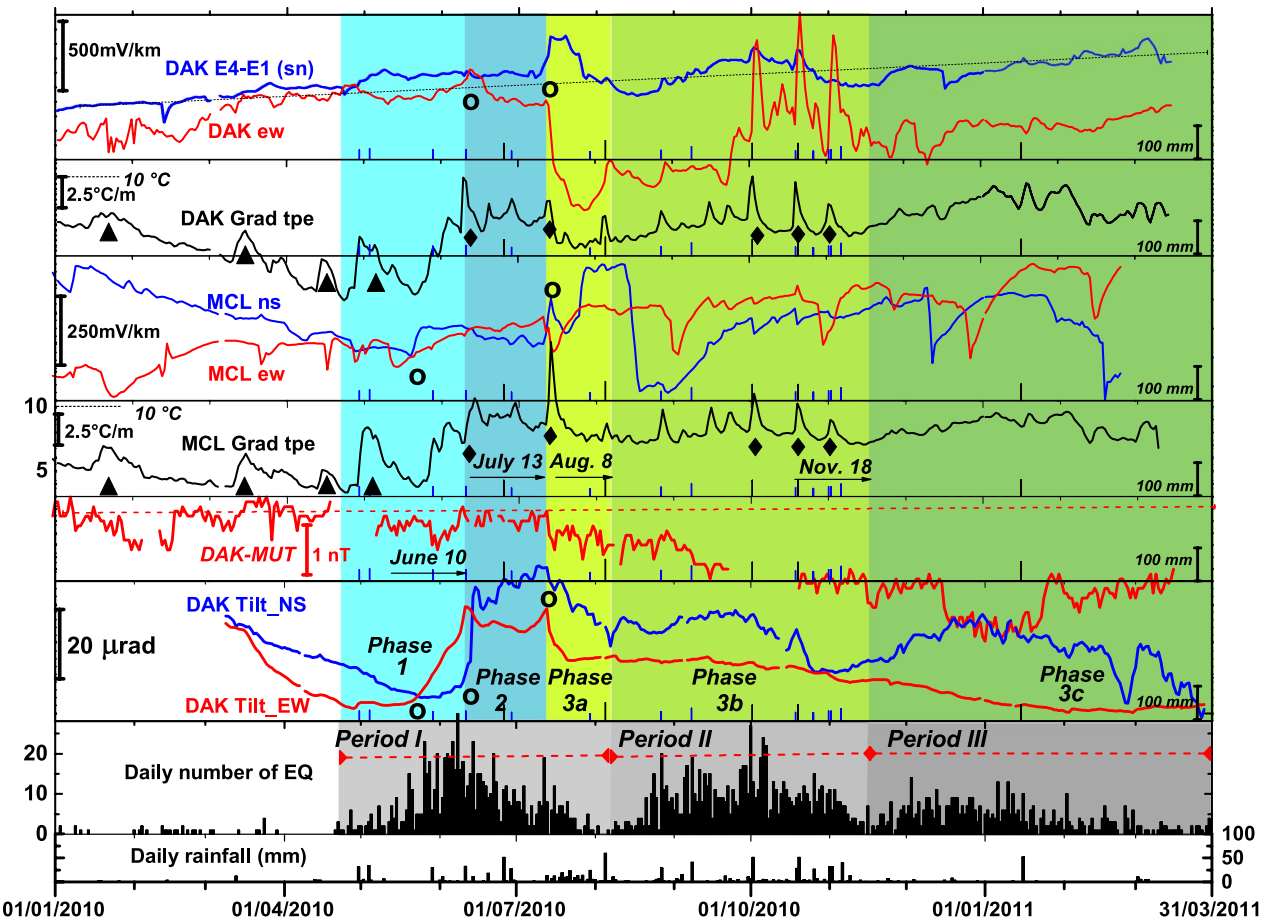

Fig. 6 Multi-parametric data recorded during the 2010 seismovolcanic crisis between January 1, 2010, and March 31, 2011. Gray boxes correspond to periods of seismic activity. Colored boxes match the different phases of tilt variations during the crisis (see text for detail). From top to bottom—Horizontal components of the electric field at DAK station (S–N, E–W), Thermal gradient at DAK, Horizontal components of the electric field at MCL station (N–S, E–W), thermal gradient at MCL, total magnetic difference [*DAK–MUT*], NS and EW components of the self-leveling borehole tiltmeter at DAK, daily number of earthquakes (PHIVOLCS document) and daily rainfall (in mm/day) at the local Buco Observatory. Black triangles represent bay-type thermal anomalies, black diamonds correspond to sharp transient thermal anomalies, and black circles figure the onset of larger common electric field and tilt signals (see text for detail). Rainfall above 25 mm (blue line) and above 50 mm (dark line) is added to each plot for comparison with single parameters

May 15 to June 11, tilt at DAK was systematically down to the east, reaching a maximum amplitude of 27.1 µrad on June 11. From June 11 to July 13, tilt at DAK was systematically down to the north, reaching a maximum amplitude of 30.3 µrad on July 13. Both components then initiated a long-term decrease back toward their respective pre-crisis levels with superimposed north–south tilt perturbations of some months duration which corresponded generally to the periods of seismicity (Figs. 5, 6, 8). Tilt had mostly recovered to pre-crisis levels when seismicity ceased in March 2011. Thus, three main phases of tilt variations occurred during the seismovolcanic crisis: Phase 1 from April 20 to June 11, Phase 2 from June 11 to July 13, and Phase 3 from July 13 to March 31, 2011.

We investigated the possibility that either temperature, or rainfall, or both might have contaminated the tilt data. On rainfall, we initially focused on the effects of the five largest rainfalls of more than 50 mm on electric field and tilt. The most important of these was the 52 mm event on Jan. 15, 2011, after most volcanic activity had ceased. This event provides a rainfall calibration that allows assessment of tilt responses in the middle of the activity to similar large rain events. We see no consistent large signals that we can ascribe to rain in the tilt data. We then looked further at the 12 rainfall events of between 25–50 mm and find these conclusions are not changed. All 17-rain events greater than 25 mm are shown on the time axes of each parameter in Fig. 6 for

easier assessment of the relevance of this issue. Furthermore, we note that since there was no rainfall between April 10 and May 1, on June 10, and between July 8 and 13, this indicates that the transient tilt signals during these times cannot be ascribed to rainfall. Furthermore, since the events coincide with changes in seismic activity, deformation and electric signals, they are most likely a consequence of activity within the volcano.

On the issue of the effect of temperature on the tiltmeter electronics, the temperature sensitivity of the tiltmeter components is (0.02% of range)/°C. The daily variation of the temperature at the depth of the tilt sensors is less that 0.1 °C peak-to-peak. Annual temperature changes at this depth are about 10 °C. Expected temperature-related tilt effects are 0.002 μrad daily and 0.2 μrad annually. At short periods (days), the primary signal we see is due to the M2 solid earth tidal loading (~0.2 μrad at a 12.4 h period) not temperature (24 h period). Observed long-term signals are far in excess of 0.2 μrad. Thus, temperature cannot be the cause of the rapid signals we observe on different sensors at the exact times of onset of new activity, although the question might be raised whether the overall loose correspondence between tilt and temperature during long periods of volcanic activity may reflect some of the longer-term changes in tilt are caused by temperature. This does not seem to be the case since, if it were true, we should have also seen large changes in tilt for the reversible changes in temperature gradient at DAK and MCL in mid-April (2.5 °C/m) and early May (~5 °C/m). Furthermore, while the increase in temperature gradient at both DAK and MCL in late May does correspond to an increase in the EW tilt component (Phase 1), it does not correspond to an increase in the NS tilt component. The temperature gradient stays flat from June 10 to July 13 (Phase 2) with short-term fluctuations but the NS component increases while the EW component decreases with fluctuations that do not occur at the same time as the gradient fluctuations.

Ground temperature and temperature gradients inside and outside the crater

Figure 5 shows the variations of the ground temperature at 80 cm depth between 2008 and March 2011. Before May 2009, the average temperatures inside and outside the crater rim at DAK and MCL were 35 °C and 42.7 °C, respectively, and annual variations were less than 3 °C. In contrast, ground temperatures reached 40.8 °C and 48 °C during the climax of seismic activity during June 2010.

From mid-2007, average thermal gradients measured at MCL indicated a decrease particularly during mid-2009 to early 2010 that reversed after March 2010 when the crisis began (Fig. 4). Compared to the average thermal gradient of 13 °C/m in July 2007, the gradient at MCL in April 2010 was 3.1 °C/m (Figs. 4, 6). Since the temperature gradient and the temperature at the deepest sensor (T80—80 cm deep) at MCL both increased from January to March 2010, it is apparent that increasing temperature at the deeper sensor is driving the gradient measurements. No significant rainfall occurred during this period. At the DAK station, the average gradient was 9 °C/m in 2009 (Fig. 4) and reduced to 0.5 °C/m during April 2010 (Fig. 6). After May 23, the average gradients at MCL and DAK increased rose to mean levels of 8.5 and 7.5 °C/m, respectively, during the seismovolcanic crisis.

During the crisis, intermediate-term (weeks) and short-term transient (7–10 days) changes in thermal gradients were observed at both MCL and DAK. Intermediate-term changes can be observed between April 24 and May 23 with gradient changes reaching 6 °C/m on May 3. Smaller changes of about 2–3 °C/m and 2–3 weeks duration occurred several times during the previous three months (see black triangles in Fig. 6). No rainfall occurred during these times. Short-term changes, characterized by sharp transient anomalies of a week to about 10 days duration, occurred on June 10 and July 13 (black diamonds in Fig. 6). No rainfall occurred during these events. Other short-term changes occurred on

(See figure on next page.)

Fig. 7 **a** Transient signals recorded at 2 s sampling rate during April 29, 2010. Upper plots are from the DAK site. Left: Horizontal components of tilt, NS (black) and EW (blue). Middle: Electric field components, SN (black) and EW (blue). Right: Ground temperature at 40 cm depth (black) and seismic RMS noise (blue). Lower plots are from the MCL site. Left: Horizontal north and east components of the magnetic field, H (blue) and D (black), respectively. Middle: Electric field components, NS (black) and EW (blue). Right: Ground temperature at 40 cm depth (black) and seismic RMS noise (blue). **b** Transient signals recorded at 2 s sampling rate during June 10, 2010. Upper plots are from the DAK site. Left: Horizontal components of tilt: NS (black) and EW (blue). Middle: Electric field components, SN (black) and EW (blue). Right: Ground temperature at 40 cm depth (black) and seismic RMS noise (blue). Lower plots are from the MCL site. Left: Horizontal north and east components of the magnetic field, H (blue) and D (black), respectively. Middle: Electric field components, NS (black) and EW (blue). Right: Ground temperature at 40 cm depth (black) and seismic RMS noise (blue). **c** Transient signals recorded at 2 s sampling rate (DAK and MCL) between July 11 and 14, 2010. Upper plots are from the DAK site. Left: Horizontal components of tilt, NS (black) and EW (blue). Middle: SN (black) and EW (blue) electric field components. Right: Ground temperature at 40 cm depth (black) and seismic RMS noise (blue). Lower plots are from the MCL site. Left: Water temperature in Main Crater Lake (15 min. sampling). Middle: Electric field components at MCL, NS (black) and EW (blue). Right: Ground temperature at 40 cm depth (black) at MCL and seismic RMS noise (blue) at DAK

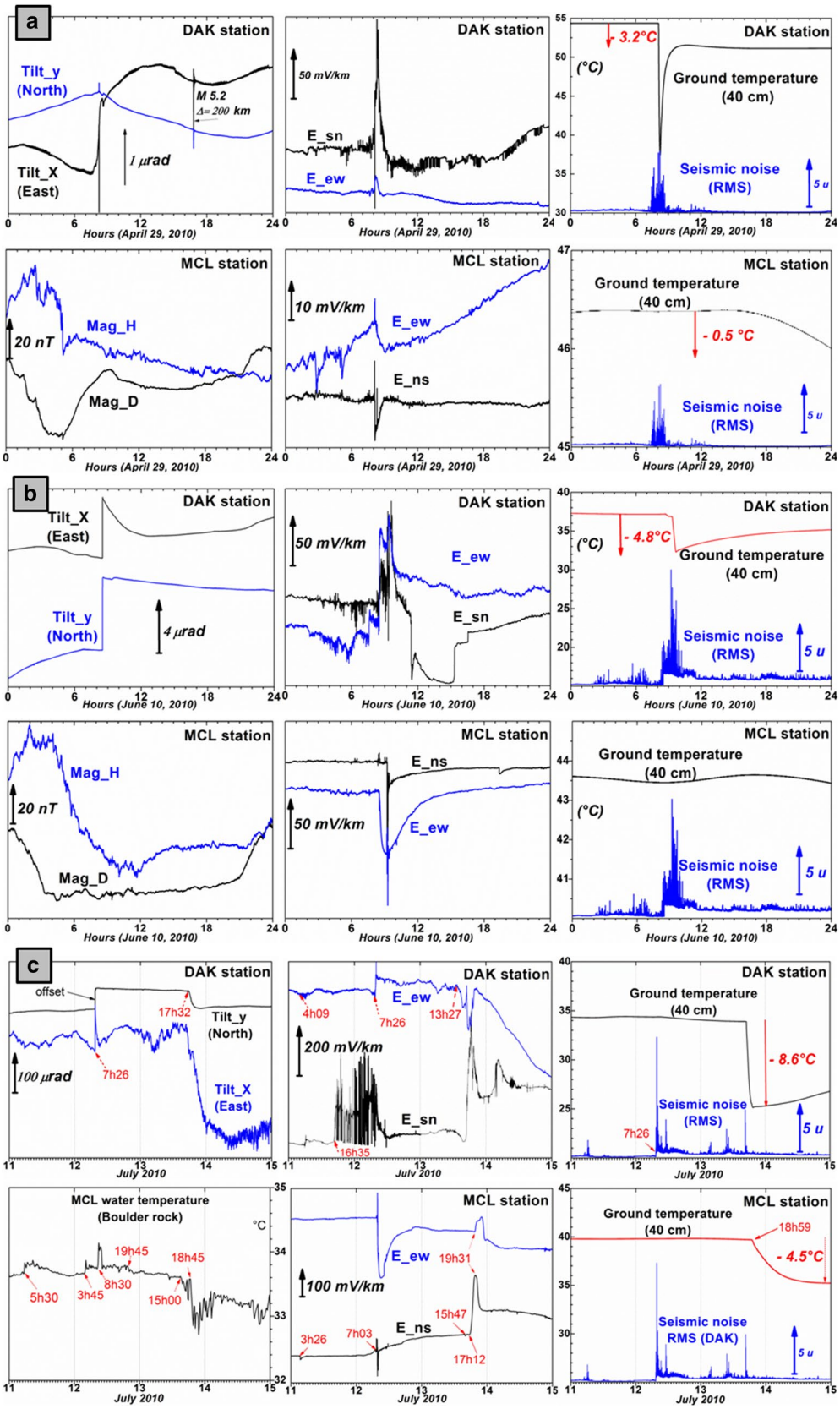
a
DAK station
Tilt_y (North)
Tilt_X (East)
M 5.2
Δ= 200 km
1 μrad
50 mV/km
E_sn
E_ew
3.2°C
(°C)
Ground temperature (40 cm)
Seismic noise (RMS)
5 u
Hours (April 29, 2010)
MCL station
20 nT
Mag_H
Mag_D
10 mV/km
E_ew
E_ns
- 0.5 °C
b
Tilt_X (East)
Tilt_y (North)
4 μrad
50 mV/km
- 4.8°C
Hours (June 10, 2010)
c
offset
17h32
7h26
Tilt_y (North)
Tilt_X (East)
100 μrad
4h09
13h27
200 mV/km
16h35
- 8.6°C
July 2010
MCL water temperature (Boulder rock)
°C
19h45
18h45
5h30
3h45
8h30
15h00
19h31
100 mV/km
3h26
7h03
15h47
17h12
18h59
- 4.5°C

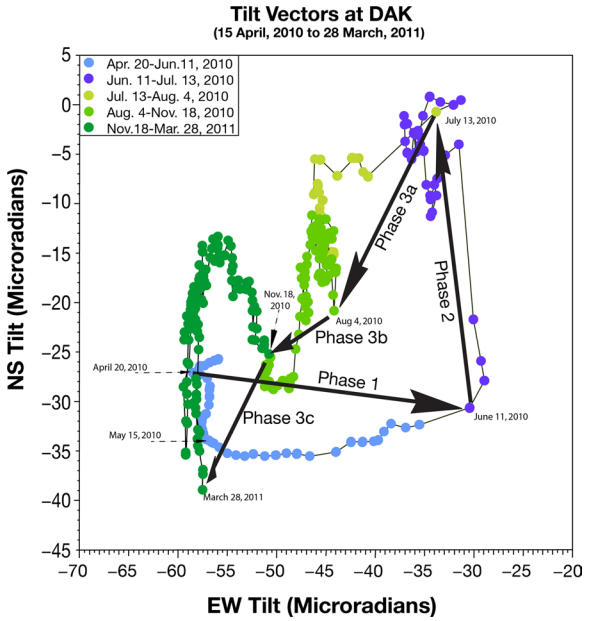

Fig. 8 Tilt vector diagram with time derived from the horizontal components of the tiltmeter located at DAK station. Black heavy vectors correspond to the main episodes of tilt between April 20, 2010, and the end of March 2011, also identified with different colors

October 1, 19 and 20 and November 1 and 2 as a result of rainfall greater than 25 mm. While these rain events were not seen on the tilt records, they did induce large rapid temperature decreases along fissures (see Fig. 5 and black diamonds in Fig. 6).

Magnetic and electric fields recorded inside and outside the crater

The magnetic field difference data [*DAK–MUT*] (Fig. 6) remained relatively flat from early October 2009 to July 13, 2010, implying that little change was observed at *DAK* during the initial stages of the 2010 crisis. From July 13, 2010, to early 2011, *DAK* decreased systematically by about 2.5 nT before starting to recover back to its 2009 baseline in early 2011. The little data that exists from [*MCE–MUT*] supports a decrease also at *MCE* of about 1 nT by late 2010.

The horizontal components of the electric field recorded at MCL and DAK between January 1, 2010, and July 13, 2011, remained generally smooth and stable (Fig. 6). After July 13, 2010, huge electric signals of 800 mV/km in amplitude were seen on both independent arrays in concert with the large temperature changes, transients in temperature gradients (see black triangles in Fig. 6) and changes observed in the tilt data at DAK signaling with the beginning of the deflation (Figs. 6, 8). We return to the question whether the electric field changes during the crisis could arise from rainfall effects. As noted above, comparison of electric field with rainfall during non-active times (Fig. 5) shows this not to be the case. Where rainfall effects are observed, they are generally small and decay quickly compared to the much larger longer-term changes observed during this volcanoseismic crisis.

Short-term transient signals

In addition to large variations in the different parameters during the main periods of the seismovolcanic crisis, short-term signals of few hours to a few days duration were independently recorded throughout the crisis at both DAK and MCL stations (Fig. 7a–c). These signals sometimes have delays from seconds up to a few tens of minutes between separated stations and appear related to changes in the volcanic activity. Examples of simultaneous tilt, magnetic, electric, temperature and seismic transient signals recorded at a 2-s sampling rate are shown in Fig. 7a–c. These effects may or may not occur with changes in swarm activity but no detailed correspondence exists between these signals and earthquake seismic waves from either local swarm activity or from larger earthquakes that are commonly recorded as seismograms on the tiltmeter. An example of a tilt seismogram from a M5.2 earthquake at 16:46 UT some 220 km to the east can be clearly seen in the tiltmeter records at 16:47 UT in Fig. 7a.

The transient signals shown in Fig. 7a–c likely result from a combination of related elastic, viscoelastic and/or hydrodynamic processes within the volcano together with more complex fluid flow models in layered porous media such as discussed by Ingebritsen et al. (2015). Unfortunately, we are not able to constrain such models with the few data we have.

The first set of events occurred on April 29, when the DAK tiltmeter showed its first large variations of about 1 μrad down to the southeast (Fig. 7a). Transient electric field signals occurred at the same time at DAK and MCL with amplitudes of 150 and 10 mV/km, respectively. Simultaneously, seismic swarm bursts were recorded at both sites together with a temporary decrease in the ground temperature of 3.2 °C in amplitude at DAK sensor located nearby one of the 1992–1994 active fissures. A smooth decrease in temperature was observed a little later at MCL. No noticeable transient magnetic change was observed at that period.

The second set of transient events were recorded on June 10 (Fig. 7b). Tilt signals at DAK indicate a rapid tilt down to the north of almost 5.5 μrad and 4.6 μrad down to the east that largely decayed during the next few hours. This was preceded and followed by changes in electric field at both DAK and MCL of up to 100 mV/

km in amplitude. The tilt changes were accompanied by increased seismic swarm noise and a decrease of 4.8 °C in the ground temperature at DAK together with smaller fluctuations in ground temperature and decreases in both NS and EW electric field components of less than 80 mV/km at MCL.

The third set of transient events occurred from July 12 to July 14 (Fig. 7c). Tilt was initially down to the north by about 80 μrad at 7:26 UT on July 12. A transient followed by a decay over several hours occurred at the same time on the east component. This was followed at 17:32 UT on July 13 by large decaying tilt down to the ESE over about 8 h. Seismic activity increased slightly on July 11 at about 5:00 UT and again at 7:26 UT on July 12. Concurrently, water temperature in *MCL* increased by 0.2 °C while disturbances in the electric fields at DAK and MCL of ~ 300 mV/km are apparent from July 11 to July 14. Step changes and decaying changes in ground temperature occurred at DAK and MCL around 18:00 UT on July 13 (Fig. 7c). Overall, this set of events on July 12–14 indicated the start of tilt recovery down to the southwest, consistent with deflation of the volcano (Fig. 6). This turning point in Taal activity was accompanied by a large temperature change in MCL, electric fields disturbances at DAK and MCL, as well as in ground temperatures inside and outside the crater (Fig. 7c).

These three sets of large and inter-correlated transient signals recorded at both DAK and MCL stations identify the start of each of three major phases in the 2010 seismovolcanic crisis at Taal Volcano: (1) the initial increase in seismicity (April 29), (2) the change within a day (June 10–11) of the tilt from an eastward to a northward direction at DAK for the next month, and (3) the beginning of the deflation of the volcano (July 13). These observations indicate that (1) the 2010 volcanic activity impacted a large part of the volcano centered on the northern part of the crater, (2) major fissures located in the northern part of *MCL*, the inner part of the crater and the main 1992–94 active fissures located in the northern geothermal field were simultaneously reactivated during major onsets of activity, and apparently are linked to processes within the volcano at depth during this time (see Zlotnicki et al. 2017).

Phases of activity and modeling

In summary, three primary episodes of seismicity, tilting, electromagnetic fields, ground temperatures and other parameters were observed during the 2010 crisis on Taal Volcano before the activity finally ended in March 2011 (Fig. 6). Within current knowledge of the existing fault structure and hydrothermal system on Taal Volcano, we now attempt to identify relatively simple but likely dynamic processes that resulted during this 2010 crisis from these multi-disciplinary data.

The three phases of activity

As discussed above, the daily number of earthquakes can be characterized by three decreasing bay-shapes periods (in gray in Fig. 6). The first period (Period I) starts on April 20, 2010, and ends between August 4 and 8. The second period (Period II) covers the period August 4–8 to November 18, and the last period (Period III) lasts from November 18 to about March 20, 2011.

The temperature gradients measured at MCL and DAK stations show a general correspondence of both shorter-term and longer-term positive anomalies occurring throughout. The shorter-term anomalies appear to occur sometimes with changes in deformation such as during the onset of the crisis on April 29, on June 10, on July 13 and August 8 (Fig. 6). Overall, the longer-term changes in thermal gradients appear to correspond generally to the three periods of seismic activity: April 29 to August 4 to 8, August 4 to 8 to November 18, and November 18 to March 2011 (Fig. 6). Both temperature gradients show hints of 3-month long variations similar to those seen in tilt and seismicity data at DAK (Fig. 6). At DAK, the periods were from May 23 to about July 25, July 25 to November 9, and from November 9 to February–March 2011. At MCL, indications of gradient change are from May 23 to about August 16, from August 16 to about November 10, and from November 10 to February–March 2011 (Fig. 6).

The components of DAK tiltmeter show three general phases of activity: Phase 1 tilting, largely down to the east from April 15 to June 11, Phase 2 tilting, largely down to the north from June 11 to July 13 and Phase 3 tilting, largely down to the southwest with superimposed episodes of north then south tilting from July 13 to March 28, 2011 (Fig. 6). This is perhaps best seen in a tilt vector diagram shown in Fig. 8 that is derived from the horizontal tilt components as a function of time. The sum of the three different tilt phases indicates apparent overall reversibility of the entire episode (black arrows in Fig. 8), since the final values reached in March 2011 were almost those during the pre-crisis period in April 2010. For simple sources at depth under the *MCL*, Phase 1 and Phase 2 would be consistent with inflation while Phase 3 after July 13 (Fig. 8) would be consistent with deflation with three sub-episodes (Phases 3a, 3b and 3c) of superimposed inflation/deflation.

During Phase 3a (light green dots in Fig. 8), tilt was initially down to the west and then down to the south. The end of Phase 3a corresponds to the end of Period I in seismic activity. Phase 3b slavishly imitates the time history of the seismic activity during Period II. Overall, one observes the persistence of the overall long-term

southwest tilt (black arrow corresponding to Phase 3b in Fig. 8) on which the sequence of north and then south tilt is superimposed (medium green dots in Fig. 8). Finally, Phase 3c (dark green dots in Fig. 8) more or less follows Period III in seismic activity (Fig. 6) with the general southwest tilt (black arrow corresponding to Phase 3c in Fig. 8) on which a north and then south tilt is superimposed. As mentioned above, both the tilt at DAK and seismicity mostly recovered to pre-crisis background levels by March 2011. The different behaviors in the tilt data appear to require the existence of at least two active sources of deformation during the crisis.

The electric field recorded at both DAK and MCL stations show that, until July 13, 2010, electric variations at DAK and MCL generally remain less than 200 mV/km in amplitude (Fig. 6) although some large variations are observed at MCL in mid-May (~ 100 mV/km) at the start of the crisis and at DAK at the peak of the crisis after June 11 (~ 200 mV/km—see black circles in Fig. 6) at the start of Phase 2. This result is consistent with suggestions that electric field changes result largely from near-surface processes. The amplitudes of the observed signals are in agreement with electric field observations on other types of volcanoes where no large eruptive events occur but where thermal ground fluids and gas move upward through fissures and geological interfaces (i.e., Hashimoto and Tanaka 1995; Michel and Zlotnicki 1998).

After July 13 (start of Phase 3), much larger short-term electric signals appear at both the DAK and MCL stations (Fig. 6). The likely reason is that these electric field changes are more sensitive to shallow triggered activity in the hydrothermal system at depths of less than 2–3 km (Zlotnicki and Nishida 2003; Aizawa 2008; Revil et al. 2008).

Modeling

Modeling of the deformation data

It is not possible to uniquely determine complex model parameters and their evolution with time with so few tilt and level line data. Nevertheless, it is possible to check for consistency between the data observed on Taal Volcano with the simplest volcanic inflation/deflation sources while also using whatever independent model constraints we can obtain to guide our choice of models and to help to understand the involved mechanisms. The leveling line data obtained by PHIVOLCS (PHIVOLCS personal communication) provide some spatial coverage but the data are infrequently sampled and the lines are short. The data indicate that inflation was observed in both data sets when the seismic activity abruptly rose in April 2010. The changes from January to July, 2010 show uplift of about 1.03 cm, 1.1 cm and 1.0 cm, respectively, along the west, north and southeast lines (PHIVOLCS personal communication). These data can be fitted with a simple inflation source at a depth of 5 km just to the northwest of *MCL* on the N120°E Regional Tectonic axis during the Phase 1 activity (Fig. 9a). This axis is along the direction of surface fissure lines discussed earlier and approximately lines up with locations of recent eruptions to the northwest (Figs. 1b, 2a, b) (i.e., Alcaraz 1966; Ramos 2001).

We use this source location and depth as the starting point of attempts to fit the observed Phase 1 tilt data since it is consistent with the simplest source necessary to produce the largely eastward tilt observed. The formulation by Davis (1986) for a pressurized prolate ellipsoid of arbitrary orientation was used for calculation of surface tilts, strains and displacements as a function of source pressure and geometry. To reduce the number of variables, the ellipsoid was assumed to be vertical (major axis "a") and the two semi-minor axes "b" and "c" were assumed to be equal in length and approximately equal in length to the semi-major axis. Thus, we have close to a simple spherical or Mogi elastic source model. We have just too few data to investigate more realistic source models that would use a layered viscoelastic medium and include effects of topography. The shear modulus was assumed to be 1 GPa. Using this model, the observed tilt at DAK during Phase 1 can be matched with a source pressure of 5 MPa located at 5 km depth, with semi-minor axes "b" and "c" equal to 1 km in directions N30°E and N120°E, respectively, and the vertical semi-major axis "a" equal to 2.5 km, as shown in Fig. 9b. We use the method of Marquardt (1963), as described in Bevington (1969), for least-square estimation of nonlinear parameters. Because of the few data we have and to be approximately consistent with the displacements indicated on the level lines, we constrain the source to be on the Regional Tectonic Axis and solve for just the position (where x-axis position is a function of the y-axis position) and the semi-major axis "a." We also carried out a grid search over the area in order to verify the validity of the inversion solutions.

(See figure on next page.)

Fig. 9 **a** Schematic showing locations of proposed sources for Phase 1 and Phase 2 under Taal Volcano and the location of tiltmeter DAK. Leveling lines performed by PHIVOLCS are shown as black dashed lines. **b** Calculated tilt at DAK during Phase 1 (April to June 11, 2010, Phase 1 in Fig. 8) from an inflation source at a depth of 5 km. The surface projection of this source is 1 km to the east of DAK. See text for source details. **c** Calculated tilt at DAK during Phase 2 (June 11 to July 13, 2010, Phase 2 in Fig. 8) from an inflation source at a depth of 2.5 km. The surface projection of this source is 1 km to the south of DAK under the *MCL*. See text for source details

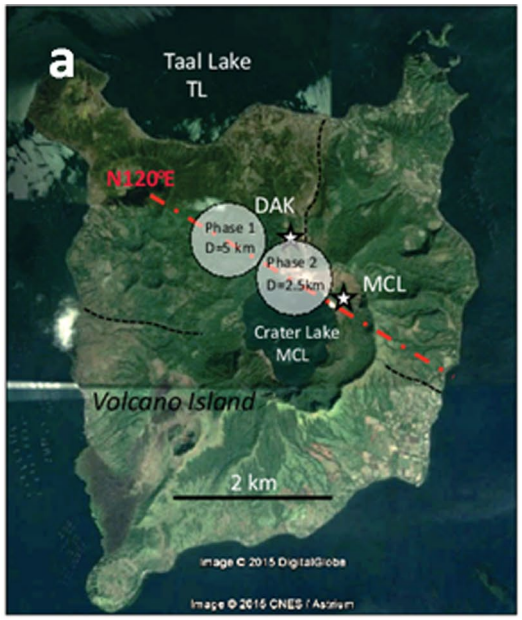
a
Taal Lake
TL
N120°E
DAK
Phase 1
D=5 km
Phase 2
D=2.5km
MCL
Crater Lake
MCL
Volcano Island
2 km
Image © 2015 DigitalGlobe
Image © 2015 CNES / Astrium

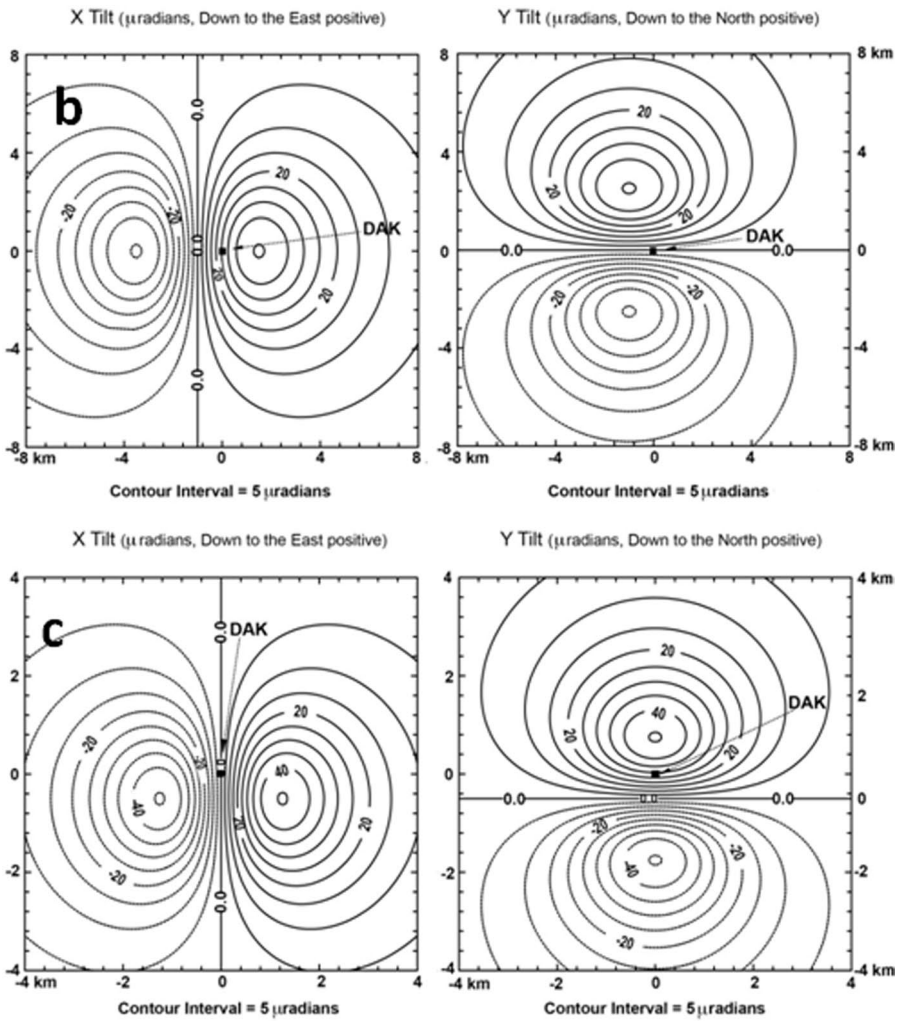
X Tilt (μradians, Down to the East positive)
Y Tilt (μradians, Down to the North positive)
b
DAK
Contour Interval = 5 μradians
X Tilt (μradians, Down to the East positive)
Y Tilt (μradians, Down to the North positive)
c
DAK
Contour Interval = 5 μradians

With so few parameters, these models serve only as a loose indication of what likely happened.

Phase 2 tilt from June 11 to July 13 cannot be explained with the same simple pressure source used to explain the tilt in Phase 1. For a simple Mogi-like volume source, uplift and NS tilting at DAK is only possible if a simple source of pressure is to the south of DAK. Since the tilting was largely down to the north, the pressure source is likely to the south in the hydrothermal system under the *MCL* where other parameters show higher activity than those outside the crater. This is still along the regional tectonic axis on the N120°E fissure line (Fig. 9a). While the source could be at a 5 km depth, other independent data suggest that it is shallower. Firstly, during this same period, the first seismic long-period (LP) events started to occur. Seismic LP events are usually associated with fluid resonance in cracks (Chouet 1992; Julian 1994) and this suggests that fluids in the hydrothermal system are the most likely cause. Second, electric data suggest activation and development of processes in the hydrothermal system largely after June 11. If the system was being pressured the most likely depth was below 2.5 km, or below the cap of the hydrothermal system as it was described by magnetotelluric surveys (Yamaya et al. 2013; Alanis et al. 2013). Third, the pulses in ground temperature gradients along the EW 1992–1994 fissures at Daang Kastila that are linked at depth in the hydrothermal system (Fikos et al. 2012; Zlotnicki et al. 2017) indicate its progressive activation with time (black triangles in Fig. 6). Again, assuming a shear modulus of 1 GPa, a search for solutions was made at about this depth. The observed tilt at DAK during Phase 2 can be matched with a source pressure of 5 MPa, depth of 2.5 km and $b=c=1$ km ("c" in the N120°E direction) with $a=1.3$ km as shown in Fig. 9c. Thus, we have the concept of two connected sources, the first deeper source (for Phase 1) feeding a second shallower source (for Phase 2) under the hydrothermal system.

After July 13 (Phase 3), both sources show overall deflation from their peak pressure of about 5 MPa from July 13 to March 2011 with three episodes of increased seismicity and tilt (Phase 3a, 3b, and 3c). The tilt perturbations indicate inflation/deflation events that are most likely from the shallower (Phase 2) source since they are observed as north/south tilting. These are likely caused by gas release, fluid transfers and other processes in the hydrothermal system (Kumagai et al. 2014). The three tilt perturbations can be modeled by transient pressure increase and decrease in the deflating Phase 2 source of about 2 MPa. The occurrence of episodes of LP seismic events, geochemical changes, electric field changes and some magnetic field changes in the hydrothermal region during Phase 3 support this concept.

Modeling of the magnetic data

With so few magnetic field data, it is not possible to uniquely determine complex model parameters and their evolution with time. However, we can investigate the degree to which different physical processes are consistent with the data. TMF data are available at *DAK* during most of the seismovolcanic crisis, but those at *MCE* are available only before the crisis and during its last stage. Some small decrease in average TMF at *DAK* is apparent from mid-May to June 10 (Phase 1), but substantial decreases do not occur until after July 13 (i.e., start of Phase 3). Even larger TMF decreases are observed during Phase 3b and 3c. Thermal demagnetization (Hashimoto et al. 2008) is one likely reason for the TMF changes. Because the thermal diffusivity of crustal rocks on active volcanoes is $\sim 10^{-6}$ m^2s^{-1}, surface thermal effects during intrusive activity are, on large scales, small and slow although they can be locally large near small scale cracks and fissures due to the transport of heat by fluid and gas. For magnetometers measuring the integrated change in magnetization with heat flow during intrusions on volcanoes, the amplitude of these signals can reach several tens of nanoTeslas (nT) over months to years (Kanda et al. 2010). Thus, these signals take a long time to emerge and usually are not in phase with the seismic activity and the rapid deformation events.

We do observe TMF changes on Taal with both rapid deformation events (hours) and with longer-term (days to months) events whose onset and recovery lag in phase with seismic and deformation events but are clearly related to the volcanic crisis. Since Taal Volcano is located at low latitude where the inclination of the geomagnetic field is 11 degrees, the thermomagnetic effects due to uniform demagnetization with heating should have increased the TMF above any newly demagnetized area. This is opposite in sign to what we observe. However, it is possible to generate thermal demagnetization signals or either sign with more complex fluid and gas flow heating sources that might be expected from gas and fluid injection into hydrothermal system but with so few data we cannot realistically explore demagnetization models.

Other possible contributing processes are electrokinetic effects (Revil et al. 2003) and piezomagnetic effects (Sasai 1991b). Electrokinetic effects result from gas and fluid flow. They should have been observed as short-term noise in the repeated SP surveys regularly made on the northern flank before the crisis. This was not the case (Zlotnicki et al. 2017). The significant magnetic fields changes we observe are progressive long-term variations. A third possible process concerns piezomagnetic effects resulting from stress changes on the magnetization of

rocks within the volcano during intrusions. Therefore, we first investigate the piezomagnetic signals in relation with the long-term TMF signals.

Analytical piezomagnetic modeling was performed with the same rigidity of the crust as in the deformation modeling (1 GPa). For such mechanically weak materials as tuffaceous rocks, stress sensitivity becomes one order of magnitude higher than for common stiff rocks (Hamano 1983; Hamano et al. 1989), and evidence of such stress sensitivity was found in the crust (Sasai 1991a). Stress sensitivity was therefore fixed to 2 GPa^{-1}. Inclination and declination of the magnetic field at Taal are 11° and 0°, respectively. Harada et al. (2005) conducted a magnetic survey over the northern geothermal field and its surroundings and obtained an average magnetization of Taal rocks equal to 5 A/m. Investigations of a number of piezomagnetic Mogi models indicate a Curie isotherm (when ferromagnetic minerals lose their magnetic properties) to be between 2 and 3 km depth. Thus, we assume an average depth of 2.5 km. This assumption of the Curie isotherm depth beneath Taal Volcano is supported by the modeling of local geothermal anomalies. Furthermore, Taal Lake belongs to "the Macolod Corridor" rift zone (Defant et al. 1988; Ohkura et al. 2001). A geothermal field known as Bulalo is located in this rift zone only 20 km east from Taal Lake. And according to geothermal well-logging, the ground temperature at the depth of 2.5 km is 320 °C which is in agreement with other estimates of Curie isotherm depths (Clemente and Villadolid-Abrigo 1993).

The lower three curves in Fig. 6 show the time variations of tilt and TMF between January 2010 and March 2011. The magnetic data show some small transitory negative changes of −0.25 nT and −0.25 nT during Phase 1 and Phase 2, respectively. A significant long-term negative trend of several nanoteslas occurs in Phase 3 from July 13, 2010, to February, 2011, with episodes during the tilt and seismicity pulses of shorter-term negative changes of −0.5 nT in Phase 3a, −0.25 nT in Phase 3b and −1.0 nT in Phase 3c. From February 2011 to late 2012 (not shown in Fig. 6), the TMF recovered to its initial state prior to the crisis.

As pointed out above, the long-term EW tilt progressively recovered at the end of Phase 3 to the level observed in April 2010 prior to the crisis. The NS tilt recovered in a similar manner but showed three successive oscillatory NS tilt changes accompanying pulses in seismicity during this recovery stage. The long-term deflation implies monotonous shrinkage of both deep and shallow sources. The three oscillatory NS tilt changes indicate episodes of inflation and deflation of the Phase 2 source whose center is 1 km to the South of *DAK*.

No analytical solution for computing the piezomagnetic field is available for the Davis' mathematical formulation of an inflated ellipsoidal cavity on a volcano (Davis 1986). Therefore, we computed TMF changes with Mogi models taking care to adjust the parameters for the different sources (Sasai 1991b). For Phase 1, the spherical source was positioned at 5 km depth with a pressure source equal to 5 MPa. The radius was fixed to 0.874 km, which gives the same volume as the ellipsoid used in the tilt modeling. For Phase 2, the same depth (2.5 km), location and source pressure (5 MPa) used in the tilt modeling were used. For Phase 3, the source pressures for the models were uniformly decreasing but positive pulses of pressure in the Phase 2 model were added and then removed. Piezomagnetic models were calculated for Phases 1 and 2 (Fig. 10—top left and right) and Phases 3a, 3b and 3c at the time of the maximum pressure changes (Fig. 10—bottom left and right). Parameters and resulting data are given in Table 1.

Computed TMF changes due to the Phase 1 source located at 5 km depth (as in the deformation model) show that only negative signals of about −0.27 nT should be expected at the *DAK* and *MCE* stations. This is consistent with the observed change in the [*DAK-MUT*] difference data of −0.25 nT (Fig. 6).

The Phase 2 modeling was computed with a source radius of 0.874 km located at 2.5 km depth. It would correspond to the location of the source within the hydrothermal system described by Alanis et al. (2013) and Yamaya et al. (2013). This model shows that we should expect −1.2 nT at *DAK*, which is in agreement with the negative sign but significantly larger than the observation (~ −0.25 nT). The discrepancy between the observation and the model could result from the fact that the simple spherical source does not take into account the elongated source in a vertical direction. Another possible reason is that the Phase 2 source is located in a non-uniform magnetic structure in which both magnetic layer material and the hydrothermal system coexist. The magnetization should be largely reduced within the hydrothermal reservoir, although we assume that it is the same in both the areas. The source has a shape of a semi-spherical cap outside of which strongly magnetized layers surround the weakly magnetized hydrothermal reservoir.

During Phase 3a, the observed data show a negative step of about −0.5 nT on about July 13 followed by a negative trend of −0.2 nT/month that continues throughout the data. The maximum signal expected from the piezomagnetic model for overall deflation in the deep Phase 1 and the shallow Phase 2 sources together with the onset

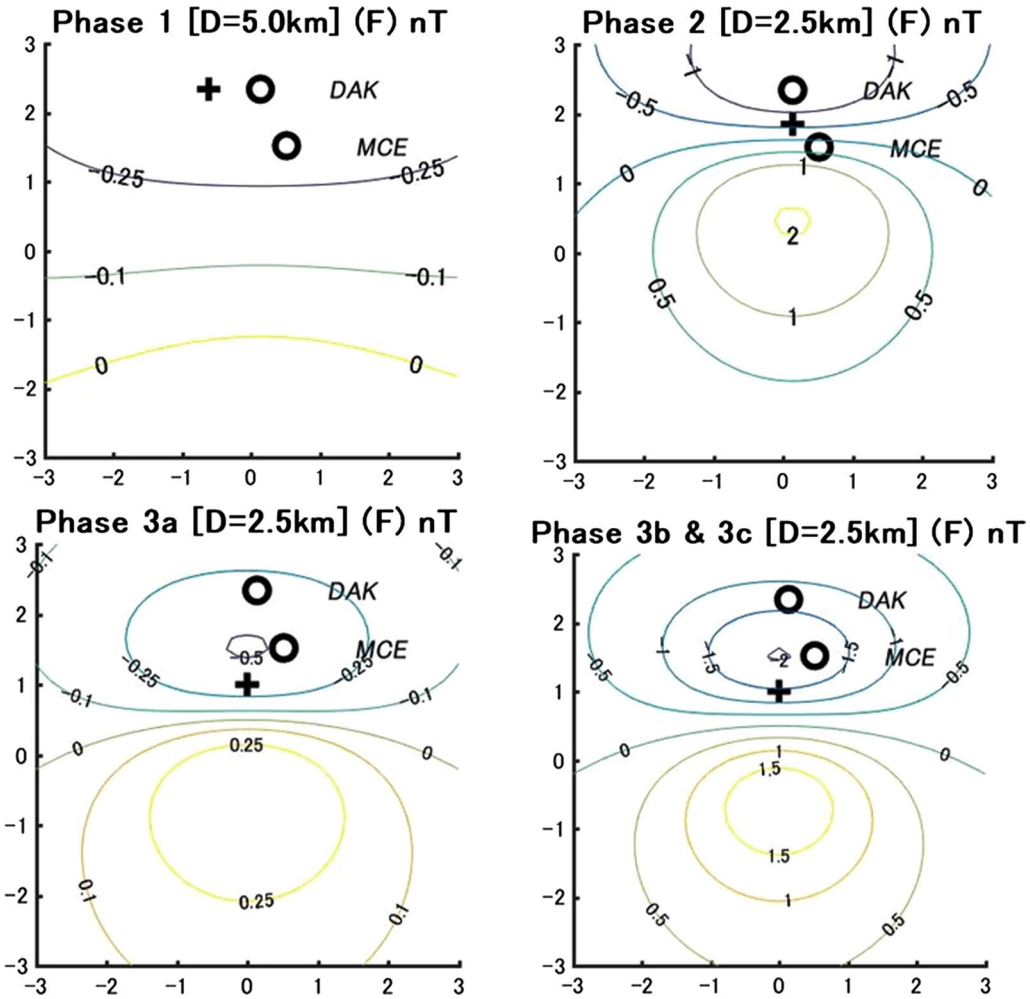

Fig. 10 Upper left: Computed piezomagnetic TMF change associated with the Phase 1 source. See text for source details. Upper right: Computed piezomagnetic TMF change associated with the Phase 2 source inflation. See text for source details. Bottom left: Computed piezomagnetic TMF accompanying an inflation pulse during overall deflation in Phase 3a. Bottom right: Computed piezomagnetic TMF change associated with inflation pulses during overall deflation in Phase 3b and 3c. In these figures, the horizontal position of each pressure source is indicated by black cross

Table 1 Model parameters of the Mogi sources and calculated TMF for Phases 1 and 2 (Fig. 10—top left and right) and Phases 3a, 3b and 3c at the time of the maximum pressure changes (Fig. 10—bottom left and right)

Phase	$x_{0\,(km)}$	$y_{0\,(km)}$	D (km)	a (km)	ΔP (MPa)	dF (DAK) (nT)
Phase 1	1.24	−0.83	5.0	0.874	5	−0.27
Phase 2	0.76	−0.01	2.5	0.874	5	−1.2
Phase 3a	1.0	0.0	2.5	1.5	0.165	−0.3
Phase 3b	1.0	0.0	2.5	1.5	0.65	−1.3
Phase 3c	1.0	0.0	2.5	1.5	0.65	−1.3

(x_0, y_0) is the horizontal location of the center of the Mogi source, D its depth, a its radius and ΔP the internal hydrostatic pressure, respectively. dF are the computed values. The origin of the horizontal coordinates is taken at (14.01°N, 121.00°E), which is located around the center of the *MCL*

of transient inflation pulse in the Phase 2 source, is shown in the lower left of Fig. 10. The calculated signal of −0.3 nT is comparable to the initially observed −0.5 nT step but if deflation is included in this solution, this calculated signal should approach zero. The ongoing negative trend in the TMF data is not accounted for.

The inflation/deflation events could result from injection of hot hydrothermal fluids into the porous materials of the external part of the hydrothermal system whose location is indicated by the magnetotelluric soundings (Yamaya et al. 2013; Alanis et al. 2013) while overall deflation was occurring. According to the 3-D model of the resistivity structure by Alanis et al. (2013), the shape of the hydrothermal reservoir is rather complicated. In computing the piezomagnetic field, we assume that the surface projection of the source sphere is located 1 km to the north of the center of the *MCL* on the N120°E Regional Tectonic axis. Spreading of the hydrothermal fluids through the reservoir is a complicated nonlinear process and the most conservative way to compute the associated piezomagnetic field is simply to estimate the piezomagnetic field due to a Mogi model which has the same size and position as the hydrothermal reservoir and gives the same tilt perturbations at DAK station during Phase 3a. The internal pressure change is estimated as 0.165 MPa (Table 1), which produces the EW tilt of 22 μrad similar to that observed at DAK (Fig. 8). The computed variation at DAK is −0.3 nT (Lower left of Fig. 10). This is slightly smaller than the −0.5 nT TMF change observed at DAK (Fig. 6). We note that the electric field at DAK changes by about 100–200 mV in the EW component at the start of Phase 2 and all components at DAK and MCL change dramatically (up to 800 mV/km) at the end of Phase 2.

The maximum signals for models that include overall deflation and intermittent inflation-deflation processes in the hydrothermal system during Phases 3b and 3c were computed with a Mogi source location at 2.5 km depth and with a radius of 1.5 km (Table 1) and are shown in Fig. 10 (Lower right). This model produces signals in magnetic field and tilt of −1.3 nT vs +15 μrad for both Phase 3b and Phase 3c, respectively. The observed signals are −0.25 nT and +15 μrad for Phase 3b and −1.0 nT vs +15 μrad for Phase 3c. The negative trend in TMF of −0.2 nT/month continues until February 2011 when it reverses and recovers to its pre-crisis level in late 2012. Thus, piezomagnetic contributions to the TMF appear to be overestimated during the Phase 3b inflation/deflation and seismicity episodes but do provide a reasonable explanation for Phase 3c. Overall, the piezomagnetic models do appear to be generally consistent with observations during Phase 1 and with inflation/deflation during Phase 3a and Phase 3c.

A different physical process appears necessary to explain the longer-term decrease (−2.0 nT from July 13, 2010, to February 2011) and increase (+2.0 nT from February 2011 to late 2012) in the TMF data that is clearly related to the volcanic crisis but is not in phase with the deformation and seismicity. Thermal demagnetization/remagnetization effects, likely a consequence of non-uniform heating and cooling when hot fluids and gas are injected into the hydrothermal system, possibly explain the long-term trend and recovery in the TMF data. We do expect these effects but cannot easily model them without detailed knowledge of the evolving plumbing system within the hydrothermal system.

The hydrothermal system is not a closed system, and is connected to the bottom of *MCL* and the northern geothermal field through multiple fissures (Harada et al. 2005; Zlotnicki et al. 2009a; Fikos et al. 2012) where increased activity was observed after June 2010 (see Zlotnicki et al. 2017). Finally, we note that the TMF at *MCE* decreased by −1 nT well in advance of the heaviest rainfall in late 2009 (Fig. 5). This also might result from thermal remagnetization although similar effects are not seen during 2008 rainfall events. Unfortunately, we do not have any continuous deformation data during this time. We note also that CO_2 degassing reached its maximum in March 2011 around the end of the Phase 3c activity (Arpa et al. 2013).

Discussion

The entire process of the 2010 seismovolcanic crisis is complex, and we have too few data to fully constrain many of the details involved. Based on calculations from relatively simple deformation models, expected effects in data from the different parameters recorded before and during the 2010 seismovolcanic crisis, the main key features of the crisis can be reviewed as follows. During the 2005–March 2010 period, the volcano showed general decreasing seismic activity although small annual seismic crises continued to be recorded. In spite of the lowering general activity, leveling surveys done by PHIVOLCS exhibited a persistent but smooth inflation with a center possibly located to the west of the northern crater rim (PHIVOLCS personal communication). We already had observed positive changes in TMF during the 2005–2006 activity of Taal (Harada et al. 2005; Zlotnicki et al. 2009a). We ascribed such changes as due to the ground temperature increase at a very shallow depth (~a few meters), because the local magnetic field also reflects thermal remagnetization (change in the magnetization of rocks with temperature) in near-surface materials (Hashimoto et al. 2008). The decrease in TMF at *MCE* by −1 nT in the middle of 2009 (Fig. 5) might be explained by rainfall cooling down the near-surface materials in the crater although the heaviest rainfall occurred from three big typhoons late in the year without obvious perturbations. This is previously discussed in Sect. 4.5 "Magnetic and electric fields recorded inside and outside the crater."

Clear deformation signals first appear on April 29, 2010 (Figs. 6, 7a, 8) when the tilt rate increased rapidly and reversed trend. Seismicity started increasing also on April

29 (see Fig. 7a) and accelerated until June 10. The deformation at this time is accompanied by the opening of fissures, short-lived decrease in ground temperatures and large transient electric signals as would be expected from reorganization of ground fluid flow. The surface temperature probably drops because, as fissures are opened in the near surface, the ground surface is cooled even though the temperature at greater depths may be increasing. The question arises regarding whether the initial trend in the tilt data indicating tilt toward the volcano should be removed. This was not done since removing the tilt rate from the entire data set prior to the activity would assume that this tilt rate is uniform and ongoing throughout the record and would skew the entire data set. Thus, we would prefer not to remove trends (when we do not know what they are due to) in order to "correct" the raw data and let the reader clearly see the rates, amplitudes and sign changes (Figs. 6, 8) occurring during the activity.

DAK tilt, as well as infrequent dry leveling surveys performed by PHIVOLCS, indicates inflation centered under the northwestern part of the *MCL* occurred in April–May 2010. Inflation processes (Phase 1) producing tilt down to the east (April to June 11, Fig. 11a) at DAK are likely due to a deep inflation source located at a depth of about 5 km. This location and depth is similar to inflation sources indicated by previous seismic and deformation crises (Lowry et al. 2001; Bartel et al. 2003; Galgana et al. 2014). Subsequent tilt (Phase 2) largely to the north (June 11 to July 13, Figs. 8, 11b) is likely due to triggered inflation at a shallower depth under the *MCL*. Both sources are located along the regional N120°E fissure line (Figs. 1b, 3a, 11a). This triggered inflation during Phase 2 probably resulted from the transfer of magmatic fluids into the hydrothermal system since LP seismic events, commonly related to the oscillation of fluids in cracks (Chouet 1992; Julian 1994), started occurring during this time.

Most probably, pressure in both the deep source at 5 km depth and the shallow inflation sources at about 2.5 km depth in the hydrothermal system reached a peak and started deflating after July 13 (Phase 3). Both overall deflation and inflation/deflation episodes (Phases 3a, 3b, 3c) apparently activated other parts of the hydrothermal system, producing seismic swarms, huge electrical signals, large changes in thermal fluxes, and transitory reopening of fissures due to fluids expansion in the porous media (Figs. 7c and 11c). This is observed most clearly in the north–south tilting and decaying seismicity data (Figs. 10d, 11c, e). This interpretation is in agreement with the conclusions from magnetotelluric soundings (Yamaya et al. 2013; Alanis et al. 2013), magnetic, self-potential (SP) mapping and electrical resistivity tomography (Harada et al. 2005; Zlotnicki et al. 2009a; Fikos et al. 2012), fluids transfers (Kumagai et al. 2014) and soil degassing surveys (Zlotnicki et al. 2009b; Arpa et al. 2013; Maussen et al. 2018). Pressure or volume change in both the deep and shallow sources apparently slowly decayed from July 13 back to about their values in May 2010. This marked the apparent end of the seismovolcanic crisis.

At the time of the crisis, no noticeable extension of the hydrothermal system was detected by self-potential surveys, in particular to the south of *MCL* (see Zlotnicki and Nishida (2003) for the methodology; Zlotnicki et al. 2017). This result means that only the two linked geothermal fields located on both sides of the northern crater rim appear to have been reactivated. Transient tilt signals, electric and ground temperatures signals related to specific events (April 29, June 10, July 11–14, and some others later) show that fissures parallel to the crater rim remain active and were broadly and simultaneously stimulated by the renewal of deep and/or shallow volcanic activity. It undoubtedly shows that the northern part of the volcano located between the active fissures in *MCL* and the limit of the northern flank geothermal field is composed of mechanically weak and mineralized materials, which could *"easily"* collapse in the crater or be involved in a future large phreatic eruption. The initial volume involved in a phreatic eruption could be indicated by the extent and depth of the largest active fissures delineating the northern geothermal field in 2010 and could be as large as 22 Mm^3 (0.6 km (EW) × 0.25 km (NS) × 0.3/2 km (deep)). This would correspond to a Volcanic Explosivity Index of 3 (Newhall and Self 1982).

A second key outcome is indicated by the dynamics of the inflation sources. The 2010–2011 seismovolcanic crisis demonstrates that rapid changes in the location and loading rate of deformation can occur rapidly (within a day) on Taal (e.g., June 11, 2010). Moreover, the 2010 seismovolcanic crisis can be considered as a mild crisis as compared to the 1992–1994 seismic crises for instance, and transfer of pressure or volume loading from the deep source (5 km depth) or the shallow source (2.5 km) in the hydrothermal system was maintained for only a month. This result should be taken into account in future eruptions scenarios and risks mitigation.

Conclusions

Since the last major eruption in 1977, Taal Volcano has shown signs of ongoing low-level activity. Almost every year, seismic crises occur and/or surface activity increases from weeks to months at a time. Following the 2005–2009 period, the activity of the volcano decreased although PHIVOLCS noticed continued smooth inflation of a few millimeters/yr. centered on the west side of the northern crater rim (PHIVOLCS personal communication). On April 20, 2010, seismic swarm activity began

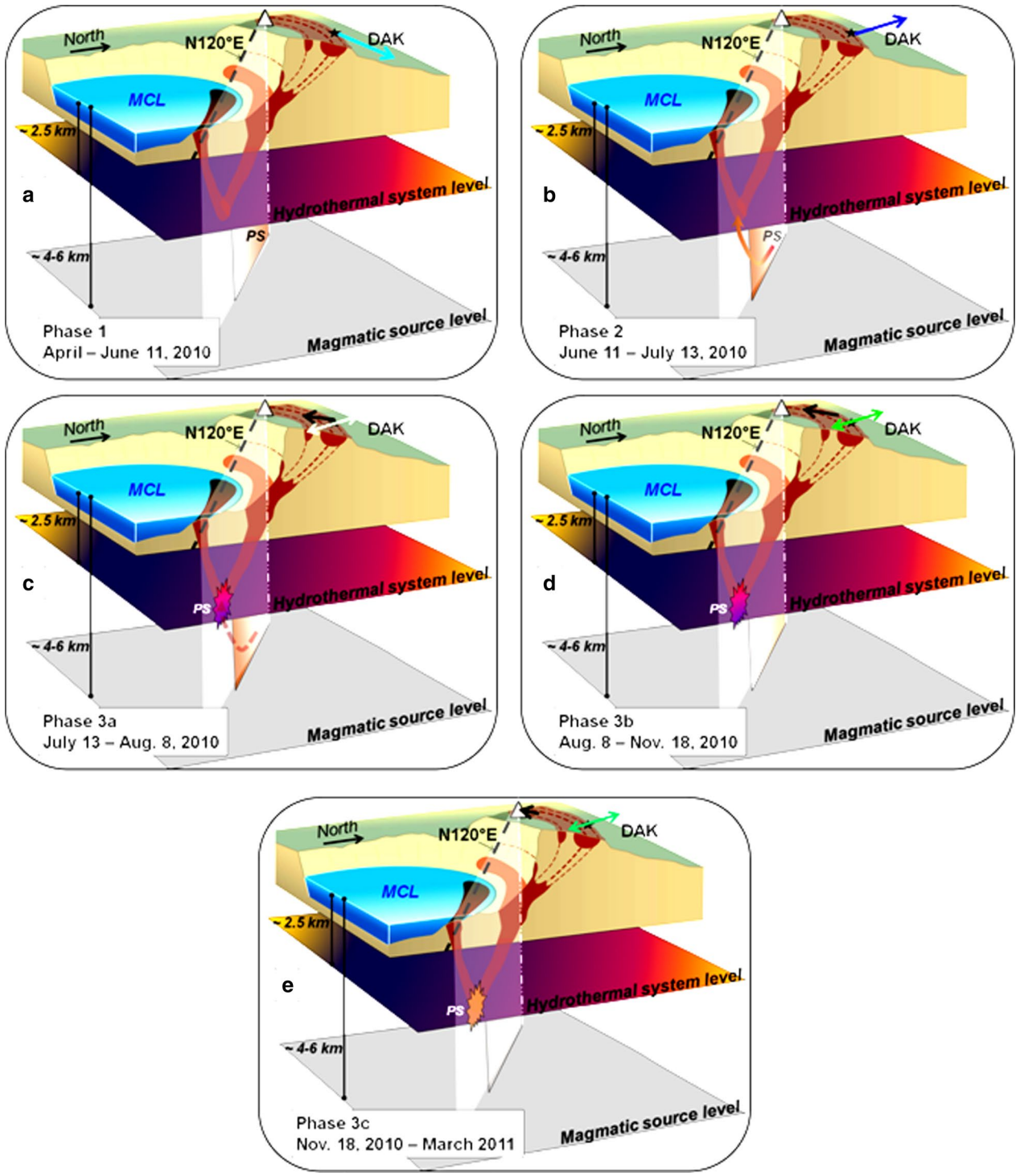

Fig. 11 Schematic interpretation of the dynamics and the source of deformation during the 2010 seismovolcanic crisis. **a** April to June 11. **b** June 11 to July 13. **c** July 13 to August 4–8. **d** August 8 to November 18. **e** November 18 to end of March 2011

again and sharply increased after April 29. The 2010 seismovolcanic crisis ended in March 2011, after three separate periods of seismic swarm activity with numbers that slowly decreased with time. The crisis was marked by violent short duration events (i.e., April 29, June 11, July 11 to 14) with opening of fissures on the north flank

of the volcano accompanied by tilts, decreases of ground temperature, and large electric field signals. These short-term events provide markers identifying different phases of activity. The first phase during the period from April 20 to June 11 corresponds to an eastward tilting of the north flank of the volcano from an apparent inflation source located at about 5 km deep and about 1 km to the west of DAK (northwest side of the crater rim). This apparently triggered Phase 2 resulting from rapid intrusion of magmatic fluids into the hydrothermal system at about 2.5 km deep under the north shore of the *MCL* during the period from June 11 to July 13. Following July 13 to March 28, 2011, the system deflated (Phase 3) back toward its pre-crisis state accompanied by pulses of inflation and deflation in the shallow source that are associated with earthquake swarms and ongoing activity in the shallow hydrothermal system where huge electric signals of several hundred of mV/km appeared after July 13, 2010.

Finally, some key lessons can be learned from this multi-parameter study of a seismovolcanic crisis. The first is the rapidity of seismic swarm onset within a few weeks with an initial intrusion activity. Second, large amplitude deformation accompanied shallow intrusions and (re)-opening of fissures outside and inside the crater (such as during July 11–14, 2010). Third, triggered intrusions can occur very quickly. Therefore, mitigation of risks should take into account the possibilities that (1) rapid depressurization during deep intrusive activity can quickly turn into phreatic eruptions, (2) surface geothermal fields and the related fissures located on both sides of the crater rim are likely connected at depth inside the hydrothermal system and can be quickly reactivated, and (3) the volume of unconsolidated materials between connected fissures inside and outside the crater could be a large fraction of the northern fracture/geothermal field and could be as much as 22 Mm^3 (0.6 km × 0.25 km × 0.15 km). This could easily involve an eruption of VEI equal to 3.

Abbreviations

CO_2: carbon dioxide; DAK: multi-parameter station located in Daang Kastila area; *DAK*: magnetometer located at DAK; EMSEV: Inter-Association on Electromagnetic Studies of Earthquakes and Volcanoes; GPS: global positioning system; MCL: multi-parameter station located inside the crater to the east; *MCE*: proton magnetometer located in the crater; *MCL*: Main Crater Lake; *MUT*: mutlinlupa magnetic station; PHIVOLCS: Philippines Institute of Volcanology and Seismology; TMF: total magnetic field; VEI: Volcanic Explosivity Index.

Authors' contributions

JZ made extensive contributions to the conception, installation and design of networks installed on Taal Volcano. He organized the acquisition of electric, tilt, and ground temperature data. He performed analysis and interpretation of the joint data. He is the lead author of the paper and has jointly written the manuscript, the revised version and made improvements in geophysical interpretation. He did important theoretical analysis. MJ made extensive contributions to conception and design of the tilt installations, acquisition of data, analysis and interpretation. He led critical discussion on ground deformation and modeling. He jointly wrote and edited the manuscript, revisions and contributed to the joint interpretation of the geophysics involved. He did central theoretical analysis. YS made crucial contributions to the conception, installation and design of magnetic network, magnetic data collection, data analysis and interpretation. He was the leading scientist working on magnetic data, modeling and interpretation. He jointly wrote and edited the manuscript, revisions and the made improvements in the interpretation. He did vital intellectual analysis. FF built and installed the electrical and temperature monitoring field equipment. He also built the data acquisition systems that have been continuously recording and automatically transferring the different data to researchers around the world for many years. He participated in the data processing and analysis of the results. EV worked from within PHIVOLCS on instrument trouble shooting, equipment operation and network maintenance. He also helped in the acquisition and processing of complementary field data. He participated to the interpretation of electric data in relation to the surface activity of the volcano. JC is a young researcher from PHIVOLCS who has greatly contributed to the collection, processing and analysis of the magnetic data. He provided complementary data for joint analysis. He coordinated periodic recovery the magnetic data and repeated measurement of the magnetic baselines during the many years of the joint cooperation. All authors read and approved the final manuscript.

Author details

[1] CNRS, OPGC-UMR6524, 24 av des Landais, 63171 Aubière Cedex, France. [2] Earthquake Prediction Research Centre, Tokai University, Shizuoka, Japan. [3] USGS, Menlo Park, USA. [4] PHIVOLCS, av. C.P. Garcia, Quezon City, Philippines.

Acknowledgements

We greatly express gratitude to the PHIVOLCS Institute, Director Renato Solidum, successive Directors of the Volcano Department, E. Corpuz, J. Sinciocco, Ma Mariton Bornas and all colleagues involved in EMSEV-PHIVOLCS cooperation for their respective contributions. These include Paolo Reniva, Loza Alan, and P. Alanis. We also greatly thank The International Union of Geodesy and Geophysics (IUGG), the International Association of Volcanology and Chemistry of the Earth's Interior (IAVCEI), the International Association of Geomagnetism and Aeronomy (IAGA), and the International Association of Seismology and Physics of the Earth's Interior (IASPEI) who have provided continuous supported for this international cooperation. The French team would like to express gratitude to the French Embassy in Manila without whose support this work could not have been completed. We also thank the Muntinlupa Magnetic Observatory for supplying magnetic data under a Memorandum of Agreement among EMSEV, PHIVOLCS, NAMRIA, ERI (Univ. Tokyo) and EPRC (Tokai Univ.) during the course of this study.

Competing interests

The authors declare that they have no competing interests

Financial support

The study was supported by: The International Union of Geodesy and Geophysics (http://www.iugg.org/), The International Inter-Association of Electromagnetic Studies of Earthquakes and Volcanoes (http://www.emsev-iugg.org/emsev/), The Philippine Institute of Volcanology and Seismology (http://www.phivolcs.dost.gov.ph/), The International Association of Volcanology and Geochemistry of the Earth's Interior (http://www.iavcei.org/), The International Association of Geomagnetism and Aeronomy (http://www.iaga-aiga.org/), The International Association of Seismology and Physics of the Earth's Interior (http://www.iaspei.org/), The French Embassy in Manila (http://www.ambafrance-ph.org/), The Observatoire de Physique du Globe de Clermont-Ferrand (http://wwwobs.univ-bpclermont.fr/opgc/).

Publisher's Note

Received: 25 June 2018 Accepted: 15 September 2018
Published online: 01 October 2018

References

Aizawa K (2008) Classification of self-potential anomalies on volcanoes and possible interpretations for their subsurface structure. J Volcanol Geotherm Res 175(3):253–268

Alanis PKB, Yamaya Y, Takeuchi A, Sasai S, Okada Y, Nagao T (2013) A large hydrothermal reservoir beneath Taal Volcano (Philippines) revealed by magnetotelluric observations and its implications to the volcanic activity. Proc Jpn Acad 89:383–389. https://doi.org/10.2183/pjab89.383

Alcaraz A (1966) Surveillance of Taal Volcano. Philipp Geol 20:1–13

Arpa MC, Hernandez PA, Padron E, Reniva P, Padilla GD, Bariso E, Melian GV, Barrancos J, Nolasco D, Calvo D, Perez NM, Solidum R (2013) Geochemical evidence of magma intrusion inferred from diffuse CO_2 emissions and fumarole plume chemistry: the 2010–2011 volcanic unrest at Taal Volcano, Philippines. Bull Volcanol 75:747. https://doi.org/10.1007/s00445-013-0747-9

Bacocol TC (2003) Etude géodésique de la faille Philippine dans les visayas. Ph.D., Université Pierre et Marie Curie, Paris, France

Bartel BA, Hamburger MW, Meertens CM, Lowry AR, Corpuz E (2003) Dynamics of active magmatic and hydrothermal systems at Taal Volcano, Philippines, from continuous GPS measurements. J Geophys Res 108(B10):2475. https://doi.org/10.1029/2002JB002194

Bevington PR (1969) Data reduction and error analysis for the physical sciences. McGraw-Hill, New York, p 336

Cardenas MB, Lagmay AMF, Andrews F, Benjamin BJ, Rodolfo RS, Cabria HB, Zamora PB, Lapus MR (2012) Terrestrial smokers: thermal springs due to hydrothermal convection of groundwater connected to surface water. Geophys Res Lett 39:L02403. https://doi.org/10.1029/2011GL050475

Chouet B (1992) A seismic model for the source of long-period events and harmonic tremor. In: Gasperini P, Scarpa R, Aki K (eds) Volcanic seismology, 3rd ed. IAVCEI Proceedings in volcanology. Springer-Verlag, Berlin, Heidelberg, New York, pp 23–97

Clemente WC, Villadolid-Abrigo F (1993) The Bularo geothermal field, Philippines: reservoir characteristics and response to production. Geothermics 22:381–394

Davis PM (1986) Surface deformation due to inflation of an arbitrary oriented triaxial ellipsoidal cavity in an elastic half-space, with reference to Kilauea volcano, Hawaii. J Geophys Res 91(B7):7429–7438

Defant MJ, de Boer JS, Oles D (1988) The western central Luzon arc, the Philippines arc: two arcs divided by rifting? Tectonophysics 145:305–317

Delmelle P, Kusakabe M, Bernard A, Fischer T, De Brouwer S, Del Mundo E (1998) Geochemical and isotopic evidence for seawater contamination of the hydrothermal system of Taal Volcano, Luzon, the Philippines. Bull Volcanol 59:557–562. https://doi.org/10.1007/s00445-012-0638-5

Fikos I, Vargemezis G, Zlotnicki J, Puertollano JR, Pigtain RC, Alanis PBK, Sasai Y (2012) Electrical resistivity tomography study of Taal Volcano hydrothermal system, Philippines. Bull Volcanol 74:1821–1831. https://doi.org/10.1007/s00445-012-0638-5

Galgana G, Hamburger M, McCaffrey R, Corpuz E, Chen Q (2007) Analysis of crustal deformation of Luzon Island, Philippines using geodetic observations and earthquake focal mechanisms. Tectonophysics 432:63–87

Galgana G, Newman A, Hamburger M, Solidum R (2014) Geodetic observations and modeling of time-varying deformation at Taal Volcano, Philippines. J Volcanol Geotherm Res 271:11–23. https://doi.org/10.1016/j.jvolgeores.2013.11.005

Hamano Y (1983) Experiments on the stress sensitivity of natural remanent magnetization. J Geomag Geoelectr 35:155–172

Hamano Y, Boyd R, Fuller M, Lanham M (1989) Induced susceptibility anisotropy of igneous rocks caused by uniaxial compression. J Geomag Geoelectr 41:203–220

Harada M, Sabit JP, Sasai Y, Alanis PKB, Cordon J Jr, Corpuz E, Zlotnicki J, Nagao T, Punongbayan J (2005) Magnetic and electric field monitoring of Taal Volcano, Philippines. Part I: magnetic measurements. Jpn Acad Sci 81B:261–266

Hashimoto T, Tanaka Y (1995) A large self-potential anomaly on Unzen volcano, Shimabara peninsula, Kyushu Island, Japan. Geophys Res Lett 22(3):191–194

Hashimoto T, Hurst T, Suzuki A, Mogi T, Yamaya Y, Tamura M (2008) The role of thermal viscous remanent magnetism (TVRM) in magnetic changes associated with volcanic eruptions: insights from the 2000 eruption of Mt Usu, Japan. J Volcan Geotherm Res 176:610–616

Ingebritsen SE, Shelly DR, Hsieh PA, Clor LE, Seward PH, Evans WC (2015) Hydrothermal response to a volcano-tectonic earthquake swarm, Lassen, California. Geophys Res Lett 42:9223–9230. https://doi.org/10.1002/2015GL065826

Julian BR (1994) Volcanic tremor: nonlinear excitation by fluid flow. J Geophys Res 90:11859–11877

Kanda W, Utsugi M, Tanaka Y, Hashimoto T, Fujii I, Hasenaka T, Shigeno N (2010) A heating process of Kuchi-erabu-jima volcano, Japan, as inferred from geomagnetic field variations and electrical structure. J Volcanol Geotherm Res 189:158–171. https://doi.org/10.1016/j.jvolgeores.2009.11.002

Kumagai H, Lacson R, Maeda Y, Figueroa MS, Yamashina T (2014) Shallow S wave attenuation and actively degassing magma beneath Taal Volcano, Philippines. Geophys Res Lett 41:6681–6688. https://doi.org/10.1002/2014GL061193

Ladanivskyy B, Zlotnicki J, Reniva P, Alanis P (2017) Electromagnetic signals on active volcanoes: analysis of electrical resistivity and transfer functions at Taal Volcano (Philippines) related to the 2010 seismovolcanic crisis. J Appl Geophys. https://doi.org/10.1016/j.jappgeo.2017.01.033

Lowry A, Hamburger M, Meertens C, Ramos E (2001) GPS monitoring of crustal deformation at Taal Volcano, Philippines. J Volcanol Geotherm Res 105:25–47

Marquardt DW (1963) An algorithm for least-squares estimation of nonlinear parameters. J Soc Ind Appl Math 11:431–441

Maso MS (1991) The eruption of Taal Volcano, January 30, 1911. Publication Weather Bureau in Manila

Maussen K, Villacorte E, Rebadulla RR, Maximo RP, Debaille V, Bornas A, Bernard A (2018) Geochemical characterisation of Taal Volcano-hydrothermal system and temporal evolution during continued phases of unrest (1991–2017). J Volcanol Geotherm Res 352:38–54

Michel S, Zlotnicki J (1998) Self potential and magnetic surveys. tools to investigate faulting, fluid circulation and eruptive dynamism of volcanoes: example of La Fournaise (Réunion Island). J Geophys Res 103(8):17845–17857

Moore JG, Nakamura K, Alcaraz A (1966) The 1965 eruption of Taal Volcano. Science 151(3713):955–960

Newhall CG, Self S (1982) The Volcanic Explosivity Index (VEI): an estimate of explosive magnitude for historical volcanism. J Geophys Res. https://doi.org/10.1029/JC087iC02p01231

Ohkura T, Nakano T, Besana GM, Sicat MJ, Hoso Y, Mangao E, Geraldo I, Daligdig JA, Ando M, Punongbayan RS (2001) GPS measurements in the Macolod corridor, Philippines. J Geol Soc Philipp 56(3–4):97–104

Pérez NM, Hernández P, Padilla G, Nolasco D, Barrancos J, Melían G, Padrón E, Dionis S, Calvo D, Rodríguez F, Notsu K, Mori T, Kusakabe M, Arpa MC, Reniva P, Ibarra M (2011) Global CO_2 emission from volcanic lakes. Geology 39(3):235–238. https://doi.org/10.1130/G31586.1

Ramos EG (2001) Geomorphic signatures of Taal Volcano. Geol Soc Philipp 56(3–4):105–124

Ramos EG (2002) Origin and geologic features of Taal Lake, Philippines. Aquat Ecosyst Health Manag 5(2):155–162. https://doi.org/10.1080/14634980290031794

Revil A, Naudet V, Nouzaret J, Pessel M (2003) Principles of electrography applied to self-potential electrokinetic sources and hydrogeological applications. J Geophys Res 104:1131–1150

Revil A, Finizola A, Piscitelli S, Rizzo E, Ricci T, Crespy A, Angeletti B, Balasco M, Barde-Cabusson S, Bennati L, Bolève A, Byrdina S, Carzaniga N, Di Gangi F, Morin J, Perrone A, Rossi M, Roulleau E, Suski B (2008) Inner structure of La Fossa di Vulcano (Vulcano Island, southern Tyrrhenian Sea, Italy) revealed by high-resolution electric resistivity tomography coupled with self-potential, temperature, and CO_2 diffuse degassing measurements. J Geophys Res 113(B07207):1–21. https://doi.org/10.1029/2007JB005394

Sasai Y (1991a) Piezomagnetic field associated with the Mogi model revisited: analytic solution for finite spherical source. J Geomag Geoelectr 43:21–64

Sasai Y (1991b) Tectonomagnetic modeling on the basis of the linear piezomagnetic effect. Bull Earthq Res Inst Univ Tokyo 66:585–722

Yamaya Y, Alanis PKB, Takeuchi A, Cordon JM Jr, Mogi T, Hashimoto T, Sasai Y, Nagao T (2013) A large hydrothermal reservoir beneath Taal Volcano (Philippines) revealed by magnetotelluric resistivity survey:

2D resistivity modeling. Bull Volcanol 75:729. https://doi.org/10.1007/s00445-013-0729-y
Zlotnicki J, Nishida Y (2003) Review on morphological insights of self-potential anomalies on volcanoes. Surv Geophys 24:291–338
Zlotnicki J, Sasai Y, Toutain JP, Villacorte EU, Bernard A, Sabit JP, Gordon JM Jr, Corpuz E, Harada M, Punongbayan J, Hase H, Nagao T (2009a) Combined electromagnetic, geochemical and thermal surveys of Taal Volcano (Philippines) during the period 2005–2006. Bull Volcanol. https://doi.org/10.1007/s00445-008-0205-2
Zlotnicki J, Sasai Y, Toutain JP, Villacorte EU, PHIVOLCS Team, Yvetot P, Fauquet F, Bernard A (2009b) Electromagnetic and geochemical methods applied to investigations of Hydrothermal/magmatic unrests: examples of Taal (Philippines) and Miyake-jima (Japan) volcanoes. Phys Chem Earth 34:394–408. https://doi.org/10.1016/j.pce.2008.09.012
Zlotnicki J, Vargemezis G, Johnston MJS, Sasai Y, Reniva P, Alanis P (2017) Very-low-frequency resistivity, self-potential and ground temperature surveys on Taal Volcano (Philippines): implications for future activity. J Volcanol Geotherm Res 340:180–197. https://doi.org/10.1016/j.jvolgeores.2017.04.020